small structures
www.small-structures.com

Recent Progress on High-Performance Cathode Materials for Zinc-Ion Batteries

Maiwen Zhang, Ruilin Liang, Tyler Or, Ya-Ping Deng, Aiping Yu, and Zhongwei Chen**

Rechargeable zinc-ion batteries (ZIBs) have emerged as a contender in the area of electrochemical energy storage applications due to their low cost and inherent safety. To optimize the battery performances, ZIBs cathode materials with high capacity and cyclability have been intensively studied, with most attention focused on traditional manganese- and vanadium-based materials. Recently, other novel cathode materials including Prussian blue analogues (PBAs), polyanions, metal sulfides, and organic compounds have begun to gain recognition as promising alternatives. These materials exhibit distinct strength such as high operating voltage, additional capacity by new redox chemistry activation, and/or highly reversible cycling process that are particularly desirable for ZIBs applications. To provide the highlight they deserve, this review focuses on introducing the recent progresses of these ZIBs cathodes and demonstrating common strategies adopted for material modification and optimization. Finally, systematic comparisons among the cathode materials are analyzed, along with challenges and perspectives on each category of the cathodes.

1. Introduction

Lithium-ion batteries (LIBs) have been the most dominant secondary energy technology of the 21st century due to their high energy density and excellent cycle life.[1–5] However, LIBs display inherent safety and environmental issues, such as thermal runaway and toxic runoff from landfill disposal.[6–8] In addition, increasing prices and supply deficits for raw metals (Li, Co, Ni, etc.) are major concerns for the long-term outlook of LIBs.[9–12] Driven by these limitations and uncertainties pertaining to LIB technologies, there has been increasing interest in investigating alternative systems based on other chemistries.[13–17] Over the past decade, there have been significant investigations toward "beyond lithium" devices such as Na^+ and K^+ batteries.[18–21] Despite the high abundancy of the two elements, their high reactivity leads to safety issues, while their large atomic radius generates difficulties in finding suitable electrode materials with high stability and kinetic performance.[22,23]

Recently, multivalent-ion (Mg, Al, Zn, Ca, etc.) batteries have garnered significant interest due to their relatively high capacity, potential cost savings, and inherent safety advantages.[24–28] However, strong electrostatic interactions between multivalent cations and their corresponding cathode host structure often lead to low reversible intercalation capacities.[29] The lack of compatible electrolytes that mitigate corrosion on the interface between the metallic anodes and current collectors is also an issue.[30] Among the multivalent metals of interest, zinc is regarded as the most promising because of its relatively low standard potential of –0.76 V versus standard hydrogen electrode (SHE), medium–high theoretical capacity of 818 mAh g^{-1} and volumetric capacity of 5855 mAh cm^{-3}.[31] Its high compatibility with aqueous electrolyte, low price, and abundancy are also highly desirable.[32]

Alkaline Zn batteries were first introduced to the market as primary batteries in the 1860s; research efforts have since been attempted to realize rechargebility with the system. However, poor cycling stability and Coulombic efficiency have rendered them with unsatisfactory performances.[33] The life-span limitation of ZIBs was significantly improved in the late 20th and early 21st centuries by breakthroughs implementing mildly acidic electrolytes that fundamentally change the redox reactions.[34–37] In the mildly acidic system, the anode redox reaction is changed to the direct conversion between Zn and Zn^{2+}, completely removing the electrochemically passive ZnO from the charge/discharge process. However, three types of cathode reactions have been reported, which include the chemical conversion reaction, the Zn^{2+} insertion/extraction, and the co-insertion/extraction of H^+ and Zn^{2+}.[30]

To date, the bottleneck for rechargeable ZIBs toward practical application remains to be the lack of cathode materials which satisfy all of the critical requirements, which include 1) morphological and crystal structure to host the highly polarized Zn^{2+} and assist the sluggish Zn^{2+} diffusion, 2) relatively high discharge capacity, 3) high operating voltage, 4) stable crystal structure to enable long-term cyclability, and 5) cost effectiveness and environmental-friendliness.[30,38] Mn- and V-based cathode materials have been the primary focus in ZIBs development,[30] and

M. Zhang, R. Liang, T. Or, Y.-P. Deng, Prof. A. Yu, Prof. Z. Chen
Department of Chemical Engineering
Waterloo Institute for Nanotechnology
University of Waterloo
Waterloo ON N2L 3G1, Canada
E-mail: aipingyu@uwaterloo.ca; zhwchen@uwaterloo.ca

The ORCID identification number(s) for the author(s) of this article can be found under https://doi.org/10.1002/sstr.202000064.

DOI: 10.1002/sstr.202000064

prior reviews have discussed the progress and key issues of these materials.[39,40] Mn-based materials are often limited by fast capacity decay due to structural instability caused by manganese dissolution and structural transformation during cycling.[33,41–46] In comparison, the stability and capacity of most V-based compounds are better than Mn-based cathodes due to higher degree of capacitive contributions and more stable crystal structures.[47–50] However, average operating voltages of most V-based compounds are around 0.75 V versus Zn/Zn^{2+}, which hinder their capability to achieve high energy density.[40,51–53]

Lately, research efforts have slowly shifted toward new classes of cathode materials, such as PBAs (Prussian blue analogues),[54,55] polyanionic compounds,[56] metal sulfides,[57,58] and organic compounds.[59] These materials have attracted interests as they exhibit advantageous characteristics that are desirable for rechargeable ZIBs cathodes. For examples, PBAs with large crystal diffusion channel present high discharge voltages (1.7–1.75 V vs Zn/Zn^{2+}), polyanions contain high abundance of structural vacancies that can aid Zn^{2+} intercalation kinetics, metal sulfides can withstand large volume expansion during cycling, and organic compounds exhibit high discharge capacity with excellent cycling performance due to their specific chemistry.[29,31,60] Although considerable works have been conducted, a systematic summary on material design and modification strategies for electrochemical performance improvement of these materials is still absent. In this work, the properties and working mechanisms of numerous ZIBs cathode materials are evaluated and reviewed. Moreover, their strengths, drawbacks and synthetic strategies, as well as a variety of suitable electrolytes are discussed. Finally, future outlook and research guidelines for developing novel ZIBs cathode materials are presented.

2. Prussian Blue Analogues

PBAs with the general formula of $MFe(CN)_6$ (M=Mo, Cu, Co, Fe, Ni, Mn, V) are also known as transition-metal hexa-cyanoferrates (MHCFs). The material family belongs to the *Fm-3 m* structural group and adopts face-centered cubic structure. Here, Fe (III) links with C atoms to form FeC_6 octahedra while M bonds with N atoms to form MN_6 octahedra, and the two octahedra are linked by cyanide (C≡N) ligands.[61,62] This crystal structure provides sufficiently large 3D diffusion channels and weak interactions with charge-carrier metal ions, which facilitates rapid ion transportation. In recent years, PBAs with merits of nontoxicity, low cost, and facile preparation have been demonstrated as promising cathode materials for monovalent metal-ion (Li^+, K^+, and Na^+) batteries[63–66] and multivalent metal-ion batteries including Al^{3+}, Mg^{2+}, and Ca^{2+}.[26,67–70] When paired with a zinc anode (–0.76 V vs SHE), operating voltages of the corresponding devices can exceed 1.5 V, which are higher than majority of available ZIBs cathode materials.[55] The type of transition metals can significantly alter the redox properties and crystal structures of PBAs, which consequently impact their electrochemical performances. For example, some may change the coordination arrangement within the crystal lattice, whereas other metals ions can contribute additional capacity as they are redox active in the operating voltage window.[71] As of now, ZnHCF, CuHCF, CoHCF, NiHCF, FeHCF, MnHCF, and multi-metal HCF have been investigated as cathodes for ZIBs.[72]

2.1. Mono-Metal Hexacyanoferrate

2.1.1. ZnHCF

In 2014, Zhang et al.[55] first applied ZnHCF (zinc hexacyanoferrate) as a cathode for ZIBs, reaching a high operating voltage of 1.7 V. They prepared rhombohedral ZnHCF via a co-precipitation method at 60 °C, which forms as the typical PBAs cubit structure experiences geometric distortion. This occurs mainly because the Zn^{2+} adopts a ZnN_4 tetrahedron instead of an octahedral configuration, which disrupts the conventional cubic structure and leads to a high abundancy of $Fe(CN)_6$ vacancies. The same group also discovered that $ZnSO_4$ electrolyte can reduce Zn dissolution from cathode commonly observed in K_2SO_4 and Na_2SO_4 electrolyte; this is likely due to the increased chemical potential of the electrolyte. The corresponding electrochemical reactions shown in **Figure 1**a can be represented as[55]

Cathode

$$x\mathrm{Zn}^{2+} + 2xe^- + \mathrm{Zn}_3[\mathrm{Fe(CN)}_6]_2 \leftrightarrow \mathrm{Zn}_{3+x}[\mathrm{Fe(CN)}_6]_2 \quad (1)$$

Anode

$$x\mathrm{Zn} \leftrightarrow 2xe^- + x\mathrm{Zn}^{2+} \quad (2)$$

X-ray diffraction (XRD) and inductively coupled plasma (ICP) results reveal that the practical Zn^{2+} intercalation number x in this formula is around 0.85. The ZIBs fabricated with ZnHCF cathode, zinc metal anode, and 1 M $ZnSO_4$ electrolyte display two main discharge plateaus at 1.75 and 1.66 V as shown in Figure 1b. The device can deliver 65.4 mAh g^{-1} at 1 C, with 76% capacity retained after 100 cycles (Figure 1c). Benefiting from its relatively high average operating voltage of 1.7 V, it delivers an energy density of 100 Wh kg^{-1} at 100 W kg^{-1}. In 2015, the same group investigated the relationship between the morphology and facet of polyhedral ZnHCF to their electrochemical performances.[60] They synthesized octahedral ZnHCF (O-RZnHCF), truncated octahedral ZnHCF (T-RZnHCF), and cuboctahedral ZnHCF (C-RZnHCF) by tuning the pipetting rate and mixing speed during the co-precipitation process, which alters the growth rate of the <100> to <111> facets. Electrochemical performances of the as-prepared samples showed that C-RZnHCF exhibits the highest rate capability and cyclic stability, whereas O-RZnHCF performs the worst (Figure 1d–g). It was also identified that C-RZnHCF particles present the largest areal percentage of F100 surface, whereas O-RZnHCF occupies the smallest. Thus, it is deduced that high areal ratio of F100 orientations is beneficial to the overall electrochemical performance. They then applied C-RZnHCF as a ZIBs cathode with 3 M $ZnSO_4$ electrolyte, which yields an average operating voltage of 1.73 V with an energy density of 104 Wh kg^{-1}.[60] In another attempt to mitigate the dissolution of ZnHCF through the common-ion effect, Ni et al. added 1 M inert Zn^{2+} into 1 M KNO_3 electrolyte. Presence of the Zn^{2+} ionic inhibitor in the electrolyte significantly enhanced

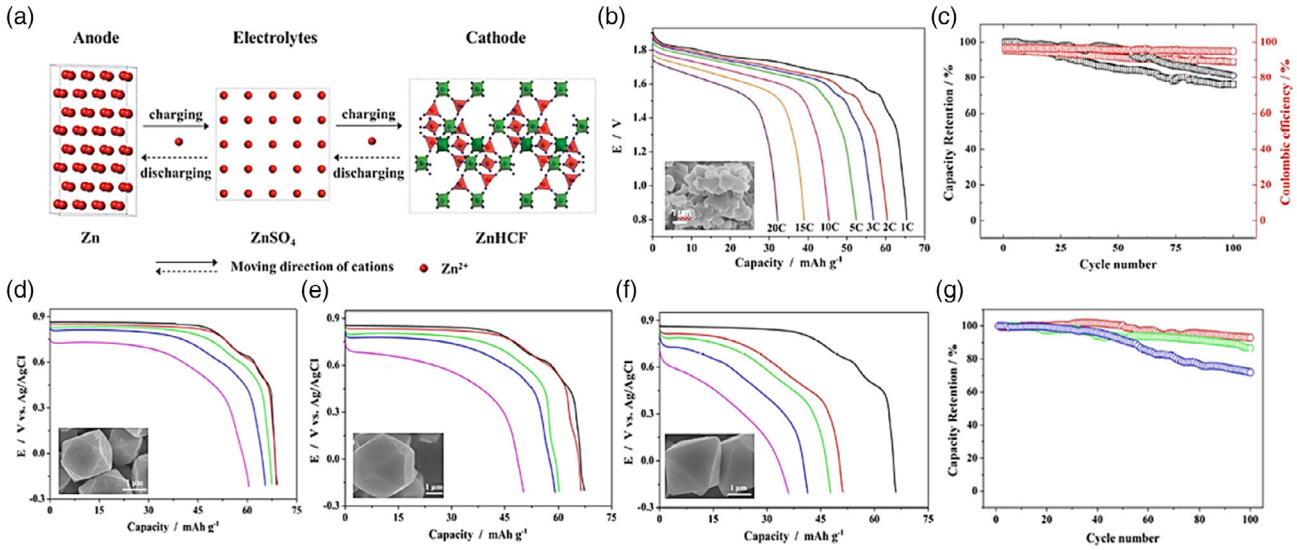

Figure 1. a) A scheme illustrating the working mechanism of ZnHCF cathode, b) rate capability, and c) 1C (square) and 5C (circle) cycling tests of ZnHCF. Reproduced with permission.[55] Copyright 2014, Wiley-VCH. Discharge curves at the rate of 1C (black), 5 C (red), 10 C (green), 20 C (blue), and 50 C (magenta) of d) C-RZnHCF, e) T-RZnHCF and f) O-RZnHCF, g) cycling stability tests of C-RZnHCF (red), O-RZnHCF (blue) and T-RZnHCF (green) by three-electrode flooded cells at 5C. 1C=60 mA g^{-1}; inset are the SEM images of different ZnHCF. Reproduced with permission.[60] Copyright 2015, Springer Nature.

the cathode capacity retention from 18% to 73.3% after 100 cycles, with 66 mAh g^{-1} at 0.3 A g^{-1} as the initial discharge capacity.[73]

2.1.2. CuHCF

Another well-known PBA ZIBs cathode is copper hexacyanoferrate ($KCuFe(CN)_6$), whose cubic framework consists of CuN_6 and FeC_6 octahedra connected by C≡N bridges. Both Wang and co-workers[74] and Mantia and Trócoli[72] synthesized highly crystalline CuHCF nanocubes with particle sizes smaller than 100 nm and studied their performance as ZIBs cathodes in $ZnSO_4$ electrolytes of different concentration and pH, where the as-prepared cathode follow the proposed reactions[72]

Cathode

$$xZn^{2+} + 2xe^- + KCuFe^{III}(CN)_6 \leftrightarrow Zn_xKCu[Fe^{III}(CN)_6]_{1-2x}[Fe^{II}(CN)_6]_2 \quad (3)$$

Anode

$$xZn \leftrightarrow 2xe^- + xZn^{2+} \quad (4)$$

From their three-electrode cyclic voltammetry (CV) results, two pairs of reversible peaks were observed corresponding to Zn^{2+} intercalation into the CuHCF structure. The mildly acidic electrolyte environment prevents the formation of ZnO and $Zn(OH)_2$ on the anode end, which is known to be a primary cause of performance degradation in alkaline systems. The fabricated ZIBs from the Mantia and Trócoli achieved 53 mAh g^{-1} or 90% of theoretical capacity, with capacity retention up to 96.3% after 100 cycles at 0.06 A g^{-1} (1 C). The cell has a high average operating potential up to 1.73 V and excellent rate capability of 81% retention from 1 to 10C.[72] Following this, the same group studied the effects of electrolyte anion pairing, electrolyte concentration, and cycling rates on the electrochemical performance of CuHCF.[75] Stability tests of ZIBs using 0.02 M $ZnSO_4$, ZnF_2, $Zn(ClO_4)_2$, and $Zn(NO_3)_2$ as the electrolyte show respective capacity retentions of 97%, 95%, 95%, and 21% after 200 cycles at 60 mA g^{-1}. The poor performance of NO_3^- electrolyte is attributed to its tendency to oxidize the zinc anode. Higher Zn^{2+} electrolyte concentration was also linked to faster copper hexacyanoferrate degradation, which was explained by the rapid occupation of the CuHCF lattice vacancies in the presence of excess Zn^{2+}, causing physical separation of the material that inhibits adequate charge transfer.[75] Recently, Mantia and Scheu et al. demonstrated the emergence of $Zn_xCu_{1-x}HCF$ wire and cubes on the cathode surface upon cycling by scanning electron microscopy (SEM), suggesting morphological conversion of CuHCF during reactions with Zn^{2+} (**Figure 2**).[76] Scanning transmission electron microscopy–energy dispersive X-ray spectroscopy (STEM–EDS), and electron energy loss spectra (EELS) of the $Zn_xCu_{1-x}HCF$ further reveal regions with rich Cu, moderate Zn, but almost no Fe adsorption, signaling the formation of $Cu(CN_6)$ and $ZnCu(CN_6)$. These two products are suspected to be inactive toward Zn^{2+} storage and thus the primary reason for the capacity degradation.

2.1.3. CoHCF

Ma et al. synthesized CoHCF as uniform nanocubes and utilized it as ZIBs cathode.[77] The material delivers a very high discharge capacity of 173.4 mAh g^{-1} at 300 mA g^{-1}, and 109.5 mAh g^{-1} at a high rate of 6.0 A g^{-1} in 4 M $Zn(OTf)_2$ electrolyte (**Figure 3**a,b), with miniscule capacity loss after 2200 cycles at 3.0 A g^{-1} (Figure 3c). The outstanding performance is attributed to proper

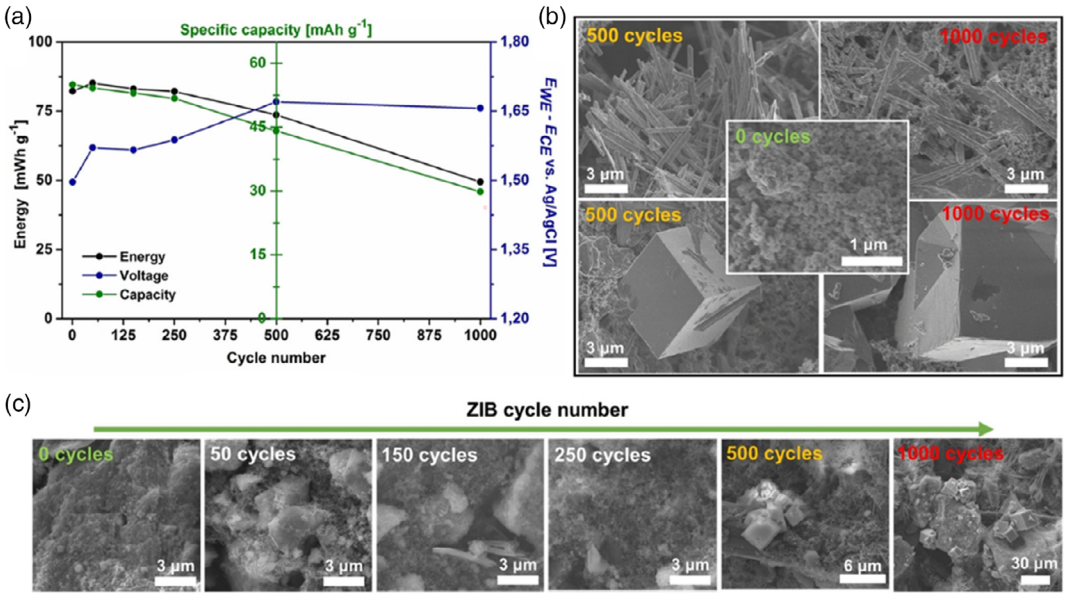

Figure 2. a) Cycling test of CuHCF cathode in 0.1 M $ZnSO_4$, b) SEM figures of wire shape and cube shape formed after 500 and 1000 cycles compared to the primary surface, c) cathode material after different cycles. Reproduced with permission.[76] Copyright 2019, Wiley-VCH.

activation of both the Co and Fe redox, which release additional capacity compared with other PBAs that only utilize the Fe redox. TEM images and STEM–EDS mapping of the cathode material were also used to confirm the well-preserved overall morphology after the Zn^{2+} storage process.

2.2. Multi-Metal Hexacyanoferrate

The electrochemical performances and mechanochemical properties of PBAs can be tuned by incorporating multiple metal ions to form mixed-MHCF.[78] One particular goal is to introduce additional redox-active sites into the cathode material to enable higher battery capacity, whereas others have reported that battery stability can be improved by suppression of undesired phase transformations.[75,79]

2.2.1. CuZnHCF

In 2019, Mantia and co-workers proposed mixed-type CuZnHCF as an alternative to CuHCF for ZIBs cathodes.[78] Different CuZnHCF mixtures can be prepared by tailoring the Zn:Cu ratio with a simple co-precipitation process at room temperature. Among them, the sample prepared with 93:7 Cu:Zn ratio shows excellent stability, with 85.54% capacity maintained over 1000 cycles at 85 mA g^{-1}, which is superior to that of CuHCF (74.3%).

2.2.2. MnCoHCF

Solanki and co-workers synthesized mixed manganese–cobalt hexacyanoferrate (MnCoHCF) with equal Mn:Co ratio and homogeneous element distribution.[80] From the three-electrode CV and galvanostatic charge/discharge (GCD) analyses, three distinct oxidation and reduction potentials were observed, and an increase in discharge capacity (111 mAh g^{-1} for MnCoHCF compared with 89 mAh g^{-1} for CoHCF at 0.025 A g^{-1}) without changes in the operating voltage was attained via partial substitution of Co by Mn. The capacity retention of MnCoHCF is 93% over 100 cycles at 0.1 A g^{-1}.

2.3. Performance Optimization Strategies

2.3.1. PBA Composites

As noted earlier, the diffusion-controlled ion-intercalation process of PBAs in ZIBs often suffers from poor rate capability. To address this issue, forming composites with other cathodes have been attempted to improve rate performance and capacity. For example, Zhang and co-workers introduced a composite where ZnHCF nanocubes are wrapped in MnO_2 nanosheets.[81] This distinct arrangement modifies the Zn^{2+} storage mechanism due to the integration of capacitive and intercalative processes by the two components, allowing the composite to achieve a high specific capacity of 118 mAh g^{-1} and an operating voltage of 1.7 V at 0.1 A g^{-1} in 0.5 M $ZnSO_4$ electrolyte (Figure 3d). As shown in Figure 3e, ZnHCF with 3D crystal framework acts primarily as the Zn^{2+} host, while the ultrathin MnO_2 sheets physically prevent structural separation. The high initial discharge capacity is due to a synergistic effect between the two components. Particularly, Zn^{2+} ions would intercalate into the MnO_2 layer and ZnHCF framework during discharge. When charged, the majority of the Zn^{2+} would be released into the void spaces between the two components, forming a Zn^{2+} reservoir at the interface of the active materials. Thus, in subsequent charge–discharge cycles, Zn^{2+} ions have a shortened diffusion path, leading to improved rate performance. This work provides a key strategy to generate PBA-based composites with promising rate capability and enhanced capacity.

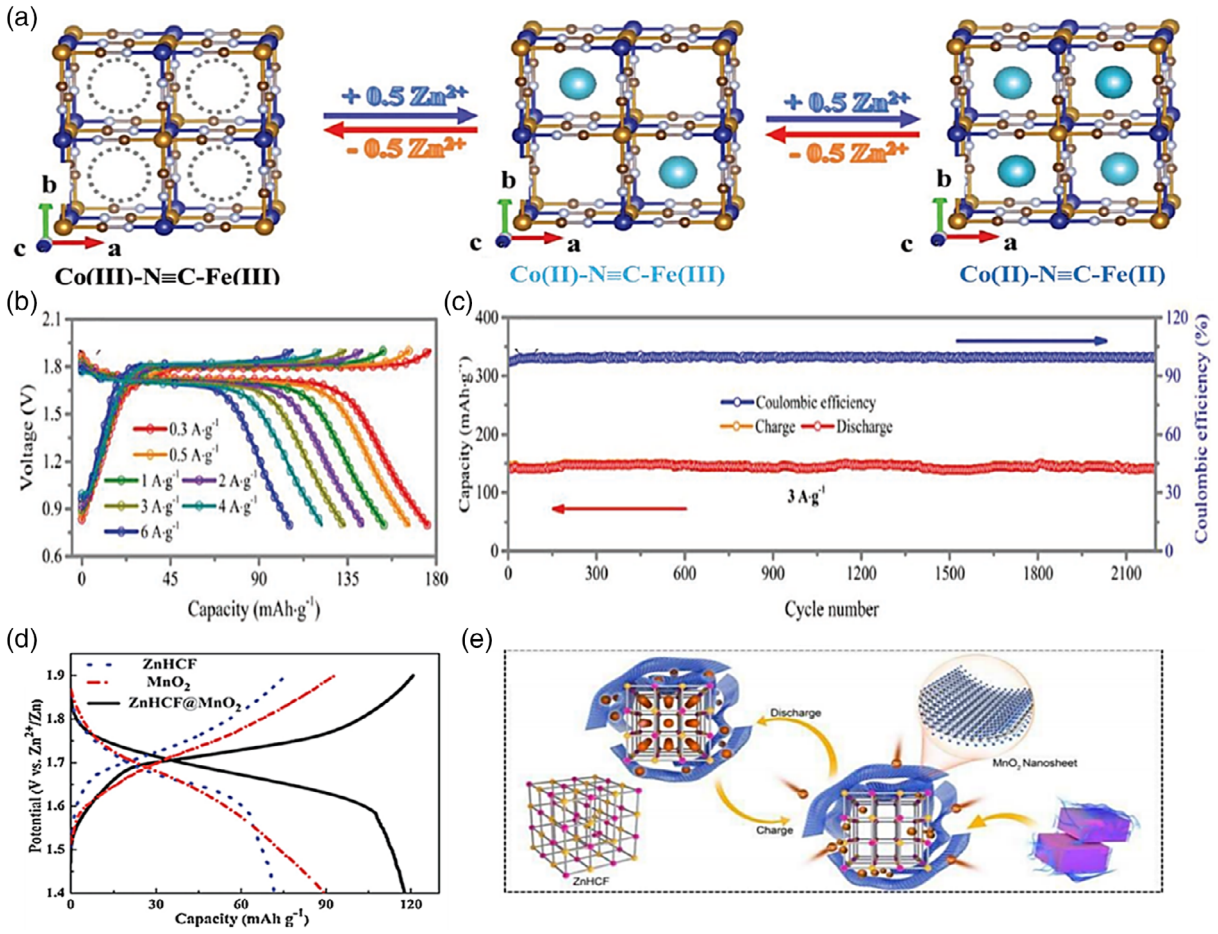

Figure 3. a) Scheme of Zn^{2+} reversible intercalation/deintercalation into CoHCF cathode with 4 M $Zn(OTf)_2$, b) GCD curves at different rates, and c) cycling stability test at 3 A g^{-1} of CoHCF. Reproduced with permission.[77] Copyright 2019, Wiley-VCH. d) GCD curves comparison of ZnHCF@MnO_2 composite and its component at 0.1 A g^{-1} and e) scheme of the ion storage process in ZnHCF@MnO_2 composite. Reproduced with permission.[81] Copyright 2017, Royal Society of Chemistry.

2.3.2. Hybrid Electrolyte

To address the issue of poor Zn^{2+} intercalation reversibility in PBA, researchers have introduced the concept of hybrid ions electrolyte in ZIBs, in which the charge-carrier ions that intercalate into the cathode have a smaller ionic radii or lower charge number than Zn^{2+}. In 2015, Steingart and co-workers cycled CuHCF against an electrodeposited Zn anode with improved electrolyte accessibility in 1 M Na_2SO_4/0.01 M H_2SO_4 electrolyte, and achieved 83% capacity retention after 500 cycles at 300 mA g^{-1}.[82] They demonstrated that Na^+ ions can intercalate reversibly into the open crystal framework of copper hexacyanoferrate, and Na^+ intercalation is preferred over Zn^{2+}, which reduces the deleterious substitution of Fe^{2+} by Zn^{2+} as previously discussed.[82] In another study, NiHCF was introduced as a cathode for ZIBs in various electrolytes (500 mM Na_2SO_4, 500 mM K_2SO_4, 500 mM Li_2SO_4 with 500 mM $ZnSO_4$ and 1 M $ZnSO_4$) with an electroplated zinc anode.[83] GCD curves of these Zn//NiHCF batteries between the voltage range of 0.9–1.9 V are shown in **Figure 4**a. Interestingly, despite having the smallest ionic radius, Li^+ ions struggle to intercalate into the channels of NiHCF due to strong ion hydration. Although the batteries using Na- and K-based electrolytes have operating voltages that are 0.2 V less than the 1.7 V of pure $ZnSO_4$, they demonstrate much higher discharge capacity. Based on the earlier results, it was concluded that Na-based electrolytes are a better choice for the Zn//NiHCF battery, which operates with a discharge capacity of 76.2 mAh g^{-1} and an average voltage up to 1.5 V, with 81% of the initial capacity retained over 1000 cycles.[83] Mantia and co-workers also adopted a similar strategy by addition of Na^+ in zinc-based electrolyte to preferentially intercalate Na^+ over Zn^{2+}, which mitigated the phase transformation of CuHCF and retained up to 82% of the initial energy density (52 mWh g^{-1}) after 500 cycles.[79]

In addition to Na^+, inexpensive nonmetallic cations such as ammonium ion have recently been proposed as the insertion ion.[84] In one study, Huang et al. utilized 1 M $(NH_4)_2SO_4$/0.02 M $ZnSO_4$ as the electrolyte with Na–FeHCF nanocubes as the cathode, which delivers a discharge capacity of 73.6 mAh g^{-1} at 0.25 A g^{-1}. Despite its remarkable cycling stability of 92.1% after 2000 cycles at 2 A g^{-1}, its low working voltage of 1.3 V is not ideal.[85] In subsequent work, the same group

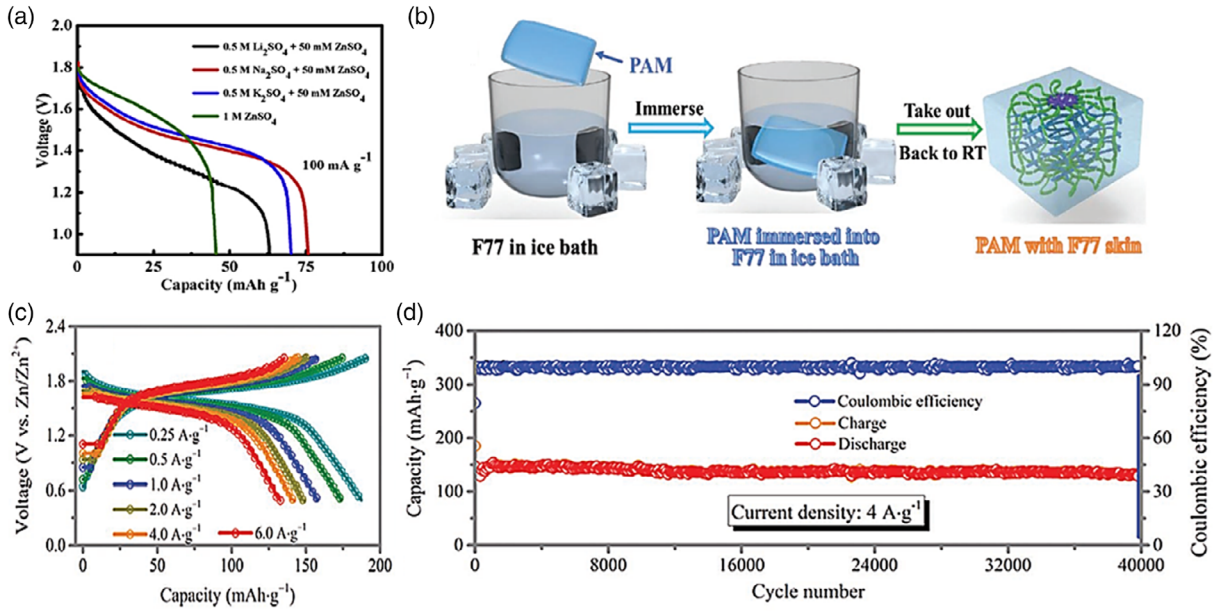

Figure 4. a) Discharge curves of NiHCF//Zn batteries in various electrolytes. Reproduced with permission.[83] Copyright 2016, Elsevier. b) Synthesis process for PAM with F77 skin hydrogel. Reproduced with permission.[77] Copyright 2019, Wiley-VCH. c) GCD curves at different rates and d) cycling performance of the fabricated CoHCF/Zn cell in ILZE at 4 A g^{-1}. Reproduced with permission.[88] Copyright 2020, Wiley-VCH.

selected CuHCF as the cathode due to its high operating potential.[86] They verified the intercalation/deintercalation of NH_4^+ by comparing the CV curves of 1 M $(NH4)_2SO_4$ and dilute H_2SO_4 at pH near 5.4. The capacitance of the cell using the diluted H_2SO_4 was negligible with no redox peaks identified, while redox peaks were obtained for the $(NH_4)_2SO_4$ cell. Using 1 M $(NH_4)_2SO_4$/0.1 M $ZnSO_4$ as the electrolyte, the constructed Zn//CuHCF cell delivers 70.4 mAh g^{-1} at 0.3 A g^{-1} and 51.2 mAh g^{-1} when ramped up to 1.8 A g^{-1}. Taking the active material mass of both electrodes into consideration, the fabricated battery achieves a satisfactory energy density of 114 Wh kg^{-1} at 458 W kg^{-1}.

2.3.3. Organic Electrolyte

Two key limitations using aqueous electrolytes in ZIBs include 1) restriction on operating voltage by their narrow electrochemical stability window, which in turn limits their energy density and 2) cathode interaction with protons or hydronium ions in acidic electrolyte, causing unexpected phase transformations and corrosion of the current collectors.[54] To avoid these issues, Hong et al. applied an organic electrolyte (500 mM $Zn(ClO_4)_2$ in acetonitrile) with $K_xNi[Fe(CN)_6]_{1-y}(H_2O)_z$ cathode in the voltage window of 0.7–1.8 V.[35] Utilization of the organic electrolyte effectively suppressed the water electrolysis side reaction commonly observed on the cathode, raising the Columbic efficiency of the cell from less than 80% with aqueous electrolyte to above 99.9% after 20 cycles. However, the overpotential and rate capability of ZIBs in organic electrolyte appear to be worse compared with their aqueous counterparts.[87] Switching to pure organic electrolytes also raises concerns toward toxicity, volatility and flammability,[88] which takes away the inherent safety advantage of ZIBs that is highly desirable in the industry.

A method to resolve the safety drawbacks of using pure organic electrolyte is to develop "bio-ionic liquid water electrolyte" through calculated mixing of aqueous and organic electrolyte. Endres and co-workers prepared rechargeable ZIBs with FeHCF nanocubes as the cathode and 1.0 M $Zn(OAc)_2$/choline acetate with 30 wt% water as electrolyte. Full cells prepared using this mixed electrolyte achieve a high capacity of 120 mAh g^{-1} with 99% Columbic efficiency at 0.01 A g^{-1}, showing that the efficiency advantage from organic electrolytes is retained without major sacrifices in battery performance.[70] When zinc powder is incorporated as the anode, the Zn/FeHCF battery delivers an energy density of 50 Wh kg^{-1}.[89]

2.3.4. Quasi-Solid-State Electrolyte

To demonstrate the practical potential of PBA-based ZIBs for wearable electronics, Zhang and co-workers fabricated a flexible quasi-solid-state cell with $ZnHCF@MnO_2$ cathode and $ZnSO_4$/PVA (polyvinyl alcohol) gel electrolyte.[81] The device reaches an energy density of 149 at 167 W kg^{-1} with capacity retention of 71% after 500 cycles. In another example, Zhi and co-workers used polyacrylamide (PAM) and F77 (poly(ethylene oxide)$_{53}$-poly(propylene oxide)$_{34}$-poly(ethylene oxide)$_{53}$) containing 4 M $Zn(OTf)_2$ as a hydrogel electrolyte.[77] Figure 4b shows the fabrication schematic of this hydrogel electrolyte, which takes advantage of the unique F77 sol–gel transition feature, where F77 is a gel at room temperature but transforms into a solution at 0 °C.[90] The battery was subjected to 0 °C treatment again upon battery construction to ensure complete gel electrolyte/active material contact. Benefiting from this optimization process, the battery achieves a high capacity of 171.64 mAh g^{-1} at 200 mA g^{-1} with exceptional capacity retention of 93.4% over 2000 cycles at

3 A g^{-1}. Worth noting, the electrochemical results of this flexible cell experience insignificant changes at bending angles of 60° and 150° or twisting deformation. Recently, the same group demonstrated a water-free quasi-solid state ZIBs by applying a [EMIM]BF_4 (1-ethyl-3-methylimidazolium tetrafluoroborate) ionic liquid with 2 M $Zn(BF_4)_2$ (zinc tetrafluoroborate) as the electrolyte (ILZE).[88] The fabricated Zn/CoHCF battery with ILZE electrolyte was charged and discharged from 0.4–2.1 V, showing slight decreases in the voltage plateaus with minor polarization. Based on the cathode mass, the battery delivers 187.3 mAh g^{-1} at a current density of 250 mA g^{-1} and retains a discharge capacity of 135.62 mAh g^{-1} at 6 A g^{-1} (Figure 4c). It exhibits outstanding capacity retention of 98% after 40 000 cycles at a rate of 4 A g^{-1} with near 100% Coulombic efficiency (Figure 4d). It is worth mentioning that the solid-state battery can endure a broad temperature range of 70 to –20 °C, and shows high tolerance toward cutting, bending, and internal exposure to ambient air.

Although PBAs exhibit promises as ZIBs cathode materials with high operating voltage up to 1.8 V, their low capacities require further improvement for consideration in practical applications. As the intercalation capacity is dependent on the number of Fe^{2+} sites accessible for reaction,[30] the unsatisfactory capacity of PBA-based ZIBs is likely associated with the incomplete activation and utilization of the multivalent ion redox.[64] Moreover, unavoidable phase transformation of PBAs upon cycling remains an issue for long-term applications of these cathodes. Overall, investigations regarding the electrochemical intercalation of Zn^{2+} in PBAs are still at their infancy. Despite successes in increasing the discharge capacity, methods to suppress PBA phase transformations during cycling still demand further investigation.

3. Polyanions

3.1. NASICONs

NASICONs stands for Sodium Super Ionic Conductor compounds, with a general formula of $A_xMM'(XO_4)_3$ (A = Mg, Na, Li etc.; M/M′ = V, Ti, Fe, Cr, etc.; X = S, Si, P, etc.). These structurally isomorphous 3D materials are highly stable due to their unique framework, which consists of large channels and excess vacancies. Their channels are favorable for metal ion intercalation, making them suitable candidates as multivalent ions hosts with enhanced ionic diffusion capability and stable cyclability.[30]

In 2016, Huang and co-workers applied $Na_3V_2(PO_4)_3$ (NVP) as an intercalation cathode material for ZIBs.[91] In this material, Na^+ ions are located at either the 18e or 6b site with different coordination environments, but only Na^+ at the 18e site can be extracted to form NVP, which offers vacancies to accommodate Na^+ or Zn^{2+} ions. The group prepared NVP nanoparticles coated by graphene-like carbon through a hydrothermal and calcination strategy to address their inherently low electronic conductivity. They then incorporated it with a Zn anode and 0.5 M $Zn(CH_3COOH)_2$ electrolyte in a battery, which delivers a capacity of 97 mAh g^{-1} between 0.7 and 1.7 V at 0.050 A g^{-1} (**Figure 5**a). It can also retain 60% of its capacity when the rate is increased to 1 A g^{-1}. Two distinct charge plateaus can be observed in the GCD curves, one at 1.40 V associated with Na^+ extraction, whereas the other at 1.25 V corresponds to Zn^{2+} extraction. However, only a single discharge plateau near 1.1 V is observed, which is attributed to Zn^{2+} insertion. From the 50 mA g^{-1} cycling test shown in Figure 5b, the battery retains 74% of its initial capacity after 100 cycles; the decay in the first few cycles is likely caused by lattice distortion as a result of Zn^{2+} insertion, which then stabilizes. Figure 5c demonstrates ex situ XRD results of the NVP cathode in its first charge–discharge cycle. As shown, a desodiated $NaV_2(PO_4)_3$ phase is found upon charging to 1.7 V and Zn^{2+} insertion phase ($Zn_xNaV_2(PO_4)_3$) appears when the battery is discharged. XPS analyses identify that the V^{3+}/V^{4+} redox was active during the charge and discharge, whereas peaks related to Zn^{2+} were also discovered confirming their intercalation into the NVP cathode. Based on the earlier results, Figure 5d shows the mechanism of Zn^{2+} insertion/extraction, which can be concluded as[91]

First charge on the cathode side

$$Na_3V_2(PO_4)_3 \rightarrow NaV_2(PO_4)_3 + 2Na^+ + 2e^- \quad (5)$$

Charge and discharge in the following cycles on the cathode side

$$NaV_2(PO_4)_3 + xZn^{2+} + 2xe^- \leftrightarrow Zn_xNaV_2(PO_4)_3 \quad (6)$$

The reactions on the anode side

$$xZn \leftrightarrow 2xe^- + xZn^{2+} \quad (7)$$

In contrast to the aforementioned study, the Mai group recently proposed that NVP exhibits simultaneous Zn^{2+} and Na^+ intercalation/extraction in 2 M $Zn(CF_3SO_3)_2$.[92] They prepared spray-dried NVP/rGO microspheres, which delivers a specific capacity of 114 mAh g^{-1} at 0.05 A g^{-1} with average voltage of 1.23 V and capacity retention of 75% after 200 cycles at 0.5 A g^{-1}. Ex situ XPS analyses of the cycled cathode detected the Na^+ signal in the initial and the first discharge state, whereas Zn^{2+} is identified after the first discharge (**Figure 6**a,b). This would support the claim that co-intercalation of Zn^{2+} and Na^+ have occurred. Ex situ XRD shows shifts of both the (116) and (113) diffractions toward lower angles when the cell is discharged to 1.2 V, which is ascribed to Na^+ intercalation (Figure 6c). When further discharged to 0.6 V, upshifts of the (211) and (113) diffractions can be observed and are attributed to Zn^{2+} intercalation. CV curves starting from the second cycle show two distinct redox peaks at 1.02/1.26 V and 1.26/1.39 V, which would align with the claim of Zn^{2+} and Na^+ co-intercalation. However, if the NVP@rGO cathode is pre-charged to 1.8 V and washed with distilled H_2O before incorporation into a cell, it loses the discharge platform near 1.3 V, as Na^+ is no longer available in the system. Based on the aforementiioned evidences, Mai et al. concluded a working mechanism of NVP/rGO, where both Zn^{2+} and Na^+ are involved in the energy storage process (Figure 6d).

Chen and co-workers designed a ZIBs using a 1 M Li_2SO_4/2 M $ZnSO_4$ hybrid electrolyte with $Li_3V_2(PO_4)_3$ (LVP) or NVP as cathodes prepared by a sol–gel method.[93] When the cells were operated between 0.7–2.1 V versus Zn^{2+}/Zn, they deliver

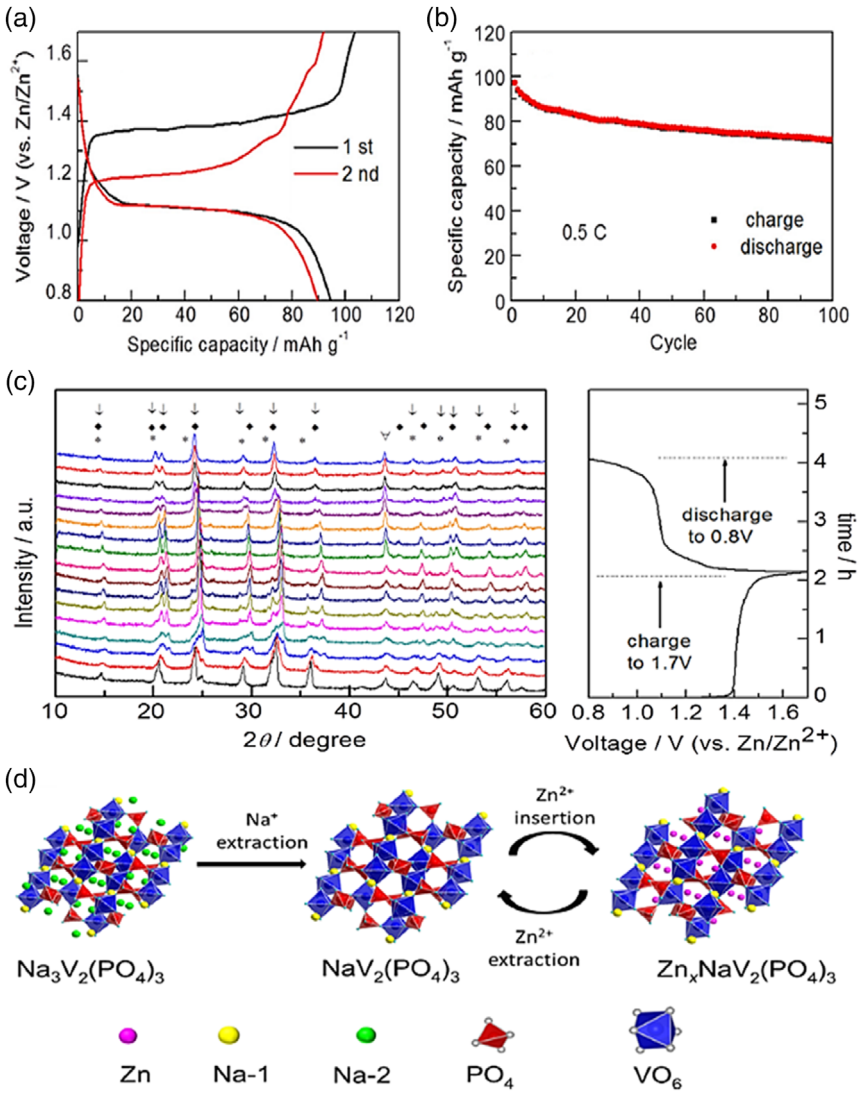

Figure 5. a) GCD curves and b) cycling tests at 0.050 A g^{-1} of the Zn//NVP battery, c) ex situ XRD patterns of NVP in a single cycle of charge and discharge, d) working mechanism schematic of NVP cathode. (*$Na_3V_2(PO_4)_3$, ↓$Zn_xNaV_2(PO_4)_3$, ◆ $NaV_2(PO_4)_3$, ∀ stainless steel). Reproduced with permission.[91] Copyright 2016, Elsevier.

capacities of 128 and 96 mAh g^{-1}, respectively, with retention up to 84% after 200 cycles. They also optimized the electrolyte pH to a range of 4.0–4.5, which were found to minimize zinc dissolution and dendrite formation in long-term cycling. In 2018, Islam et al. applied 2 M $NaCH_3COO$/1 M $Zn(CH_3COO)_2$ as the electrolyte with carbon-wrapped NVP composite as the cathode.[94] The nanoparticles wrapped with carbon results in a high surface area, enhancing active material utilization. Furthermore, the nanoparticles allow for shortened Na^+ diffusion path, whereas the carbon matrices limit particle aggregation and ensure electronic percolation, and thus the composite is capable of delivering a capacity of 66 mAh g^{-1} at a high rate of 3.7 A g^{-1} and retaining 72% capacity after 1000 cycles. From these studies, the use of hybrid electrolyte with Li^+ or Na^+ as the intercalating ion is proven to successfully mitigate the volume expansion commonly observed with Zn^{2+} intercalation, which can be an effective strategy to prevent structural degradation and extend the life span of LVP/NVP cathodes.

3.2. $VOPO_4{\cdot}nH_2O$

Layered $VOPO_4{\cdot}nH_2O$ with adjustable interlayer spacing for the intercalation of multivalent cations can be prepared by a simple low-temperature synthesis method.[40] It is an ideal cathode material because the water molecules existing between the metal phosphate layers can decrease the electrostatic repulsion among the intercalated Zn^{2+} and ease ion migration within the host structure.[95]

In 2019, Chen and co-workers demonstrated oxygen redox processes in layered $VOPO_4$ cathode with concentrated 21 M LiTFSI/1 M $Zn(Tr)_2$ "water-in-salt" electrolyte, which restricts free movement of water and thus suppresses oxygen evolution

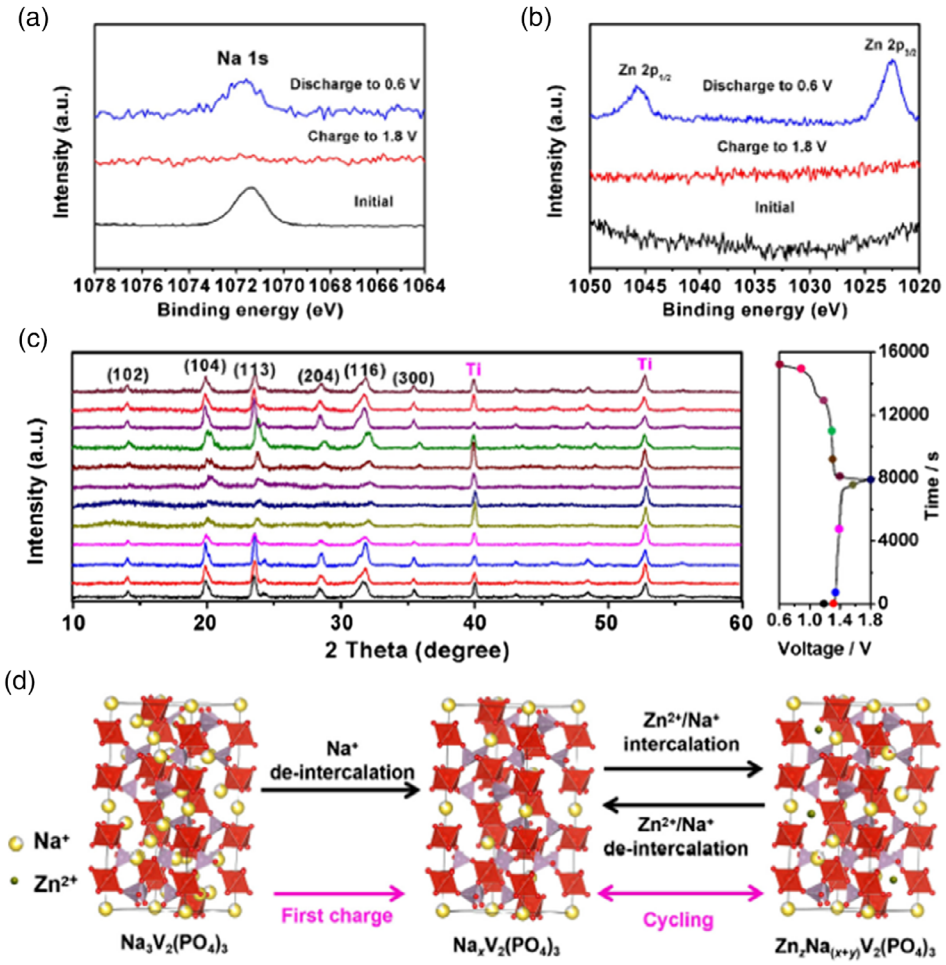

Figure 6. XPS results of a) Na 1s, b) Zn 2p of the NVP@rGO in different stages, c) ex-situ XRD spectra of NVP@rGO during charge/discharge process at 0.1 A g^{-1}, d) scheme of the (de-)intercalation process in NVP@rGO. Reproduced with permission.[92] Copyright 2019, Elsevier.

up to 2.6 V.[96] In contrast to traditional ZIBs, these Zn/$VOPO_4$ batteries were first charged to 2.1 V, which exhibits an obvious plateau (**Figure 7**a). XPS results indicate that O^{2-} was oxidized to O^- during this process, and the reverse occurred in the following discharge from 2.1 to 1.7 V. The initial, discharged and charged states of the cathode were further analyzed with ex situ XPS, XRD, SXAS (soft X-ray absorption spectra), K-edge XANES (K-edge synchrotron X-ray adsorption near-edge structure), and density of states (DOS) calculation (Figure 7b). The analyses reveal that the DOS of O^{2-} and V^{5+} can overlap when the battery is charged above 1.7 V, which activates the lattice O^{2-}/O^- redox by electron donation to the overlapping V^{5+} orbitals. This oxygen redox reaction does not interfere with the cathode reactions below 1.7 V, which operates primarily with Zn^{2+} insertion and extraction. Successful activation of the lattice oxygen redox by raising the cap voltage to 2.1 V increases the average operating voltage up to 1.56 V, boosting the energy density of the corresponding ZIBs from 160 (0.8–1.8 V) to 217 Wh kg^{-1}. Overall, the energy-storage mechanism of layered $VOPO_4$ cathode (Figure 7c) in concentrated 21 M LiTFSI/1 M $Zn(Tr)_2$ can be illustrated with the following electrochemical reactions[96]

Cathode

$$Zn_xVOPO_4 \leftrightarrow VOPO_4 + xZn^{2+} + 2xe^- \quad (8)$$

$$VOPO_4 \leftrightarrow VO^{\gamma+}PO_4 + \gamma e^- \quad (9)$$

Anode

$$\left(x + \frac{\gamma}{2}\right)Zn^{2+} + (2x + \gamma)e^- \leftrightarrow \left(x + \frac{\gamma}{2}\right)Zn \quad (10)$$

Serious performance degradation of $VOPO_4{\cdot}nH_2O$ in aqueous electrolyte upon cycling have previously been reported by Sun and co-workers, who identified that decomposition to VO_x and PO_4^{3-}, and subsequent release to the electrolyte are the primary cause of decay (Figure 7d).[97] To resolve the issue, a 13 M $ZnCl_2$/0.8 M H_3PO_4 mixed electrolyte was applied, in which the PO_4^{3-} ions alter the decomposition/dissolution equilibrium, whereas the highly concentrated $ZnCl_2$ salt prevents $VOPO_4{\cdot}nH_2O$ dissolution and suppresses oxygen evolution. The prepared cell achieves high specific capacity of 170 mAh g^{-1} at a voltage

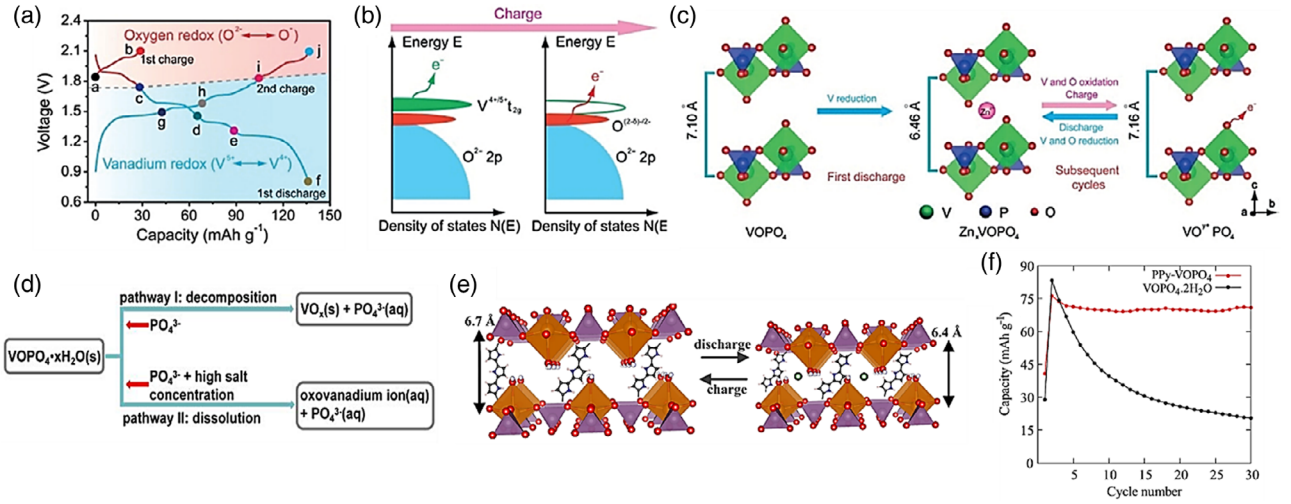

Figure 7. a) GCD curves of Zn/$VOPO_4$ cells at 50 mA g^{-1}, b) DOS analysis of $VOPO_4$, c) scheme of oxygen and vanadium redox working mechanism in $VOPO_4$ during cycling. Reproduced with permission.[96] Copyright 2019, Wiley-VCH. d) Proposed $VOPO_4$ degradation paths in aqueous solutions. Reproduced with permission.[97] Copyright 2019, Wiley-VCH. e) Scheme of PPy-$VOPO_4$ working mechanism and f) cycling test of PPy-$VOPO_4$ and $VOPO_4$ at 0.1 A g^{-1}. Reproduced with permission.[95] Copyright 2019, American Chemical Society.

window of 0.7–1.9 V with high Columbic efficiency, and maintains both stable capacity and high voltage over 500 cycles.

3.3. Performance Optimizing Strategies

To further improve the lattice stability of NVP, researchers have also incorporated F atoms to form $Na_3V_2(PO_4)_2F_3$ (NVPF), which utilizes the strong electronegativity of F^- to ensure rigid bonding of the framework.[98] For example, Jiang et al. applied NVPF as a ZIBs cathode and showed that it shares a similar Zn^{2+} storage mechanism as NVP.[99] They discovered that NVPF is converted to $NaV_2(PO_4)_2F_3$ in the first charge, following which, 0.5 Zn^{2+} ions can be inserted into the framework during discharge, forming $Zn_{0.5}Na_2V_2(PO_4)_2F_3$. Zn^{2+} ions can then be shuttled reversibly in the subsequent cycles. Using a NVPF cathode and Zn foil roll-coated with carbon black layer as the anode, the fabricated ZIBs operated at a high working potential of 1.62 V with superior cycling stability, retaining 95% capacity after 4000 cycles at 1 A g^{-1}.

Recently, Srinivasan and co-workers intercalated polypyrrole between the crystallographic layers of $VOPO_4$, which can serve as better pillaring units compared to water molecules (Figure 7e).[95] As shown in Figure 7f, a clear improvement in cyclability is achieved with the incorporation of polypyrrole to the crystal structure. The researchers also optimized the ratio of water in organic electrolyte by finding a balance between using higher water content to promote Zn^{2+} desolvation on the electrode–electrolyte interface and low water content to restrict cathode dissolution. Upon systematically evaluating the different options, they chose 1 M $Zn(CF_3SO_3)_2$/acetonitrile with 10 vol% water as the electrolyte and the prepared ZIBs demonstrates an extended life span over 350 cycles with an operation voltage of 1.1 V.

In summary, polyanions such as NASICONs and $VOPO_4$ have been discovered as ZIBs cathodes with suitable channels and interlayers. Aside from Zn^{2+} intercalation, these materials also showed compatibility with co-intercalation of other ions or lattice oxygen redox, which provides a path toward higher electrochemical performance. Currently, the phase-transformation mechanisms of these materials have not been completely uncovered, so further explorations may lead to interesting findings given the flexibility of their chemistry.

4. Metal Sulfides

Layered transition-metal dichalcogenides have received considerable attention due to their graphene-like layered structure that enables rapid ion diffusion and direct bandgap that enables facile electron hopping between orbitals. These characteristics make them promising candidates as electrodes, where they have already been applied as electrodes for LIBs and SIBs.[100] Their structures bonded through weak van der Waals forces enable rapid transportation of charge carriers and provide enough strength to withstand volume changes during multivalent ion (de-)intercalation.[58]

4.1. Vanadium Sulfides

Mai and co-workers were the first to apply VS_2 nanosheets as cathodes for ZIBs in $ZnSO_4$ aqueous electrolyte.[58] In the crystal structure of VS_2, each V atom is surrounded by six S atoms linked by covalent bonds. During discharge, Zn^{2+} is intercalated into the VS_2 framework where the process can be divided into the conversion of VS_2 to $Zn_{0.09}VS_2$ from 0.82–0.65 V, followed by an additional phase transition to $Zn_{0.23}VS_2$ between 0.65–0.45 V. When the battery is charged, Zn^{2+} ions are extracted and the structure steadily returns to VS_2. This VS_2 cathode can deliver 190.3 mAh g^{-1} at 0.05 A g^{-1} and retains 98% of its capacity after 200 cycles. Ex situ TEM and XRD analysis show that the interlayer space of VS_2 can comfortably accommodate Zn^{2+} insertion,

with minimal expansion of 1.73% along the *c*-axis accompanied by minor shrinkage along the *a*-axis and *b*-axis. The proposed electrochemical reactions of the VS_2 cathode are

$$VS_2 + 0.09Zn^{2+} + 0.18e^- \leftrightarrow Zn_{0.09}VS_2 \quad (11)$$

$$Zn_{0.09}VS_2 + 0.14Zn^{2+} + 0.28e^- \leftrightarrow Zn_{0.23}VS_2 \quad (12)$$

In 2018, VS_4 with V^{4+} and disulfide ligands $(S—S)^{2-}$ formed in a chain-like crystal structure was coupled with rGO through a hydrothermal approach by Wang and co-workers.[101] This VS_4/rGO composite demonstrates the capability to host reversible Zn^{2+} intercalation in 1 M $Zn(CF_3SO_3)_2$. When evaluated as cathode for ZIBs, it achieves a high capacity of 180 mAh g^{-1} at 1 A g^{-1} and capacity retention of 93.3% after 165 cycles. The composite also displays high rate capability, maintaining 83.7% of its capacity when the rate is increased from 0.2 to 2 A g^{-1}. The study attributed the excellent performance to the VS_4 crystallographic structure with large open tunnels suitable for rapid ion intercalation, combined with the elevated conductivity from rGO. The proposed reaction mechanism of the composite consists of intercalation from VS_4 to Zn_xVS_4 and a conversion reaction from VS_4 to $Zn_3(OH)_2V_2O_7{\cdot}2H_2O$ and S.

Researchers have also composited V_3S_4 with hydrophilic and carbonaceous substrates (hcc), which consist of CNTs, carbon fibers, and acid-treated natural halloysite to form complex cathodes for ZIBs.[102] The choice of carbon substrate is specifically selected to enhance the conductivity and reaction kinetics of the sulfide, especially the acidified halloysite and CNTs with high conductivity and hydrophilicity are expected to aid charge and mass transport for the redox process. When incorporated into ZIBs, the hcc-V_3S_4 demonstrates a discharge capacity of 148 mAh g^{-1} at a rate of 500 mA g^{-1}.

4.2. Performance Optimizing Strategies

Compared to other ZIBs cathodes, the standard interlayer distance of MoS_2 is 3.1 Å, which is too narrow for Zn^{2+} hydrate (5.5 Å) intercalation. To resolve this problem, Liang et al. demonstrated a hydrothermal reaction to incorporate oxygen to the MoS_2 framework (MoS_2—O), which tunes both the material hydrophilicity and the interlayer spacing.[103] It is suggested that the shorter Mo—O bonds and electronegative O atoms can weaken the van der Waals attraction between the MoS_2 layers, and thus expand the interlayer spacing to 9 Å (**Figure 8**a). Moreover, the incorporation of oxygen also lowers the intercalation energy barrier of MoS_2 and transforms it into an efficient storage material. As a result of the modification, MoS_2—O exhibits a high specific capacity of 232 mAh g^{-1} at 0.1 A g^{-1}, showing great improvement compared to the 21 mAh g^{-1} for MoS_2 (Figure 8b). Worth noting, the diffusivity of Zn^{2+} ions in MoS_2—O was also increased by three orders of magnitude compared to pristine MoS_2. In another study, Zhi and co-workers prepared MoS_2 nanosheets with expanded interlayer spacing (0.7 nm) vertically aligned on a carbon cloth scaffold.[104] The freestanding MoS_2 structure enhances the interfacial contact with the electrolyte and the expanded layer distance of MoS_2

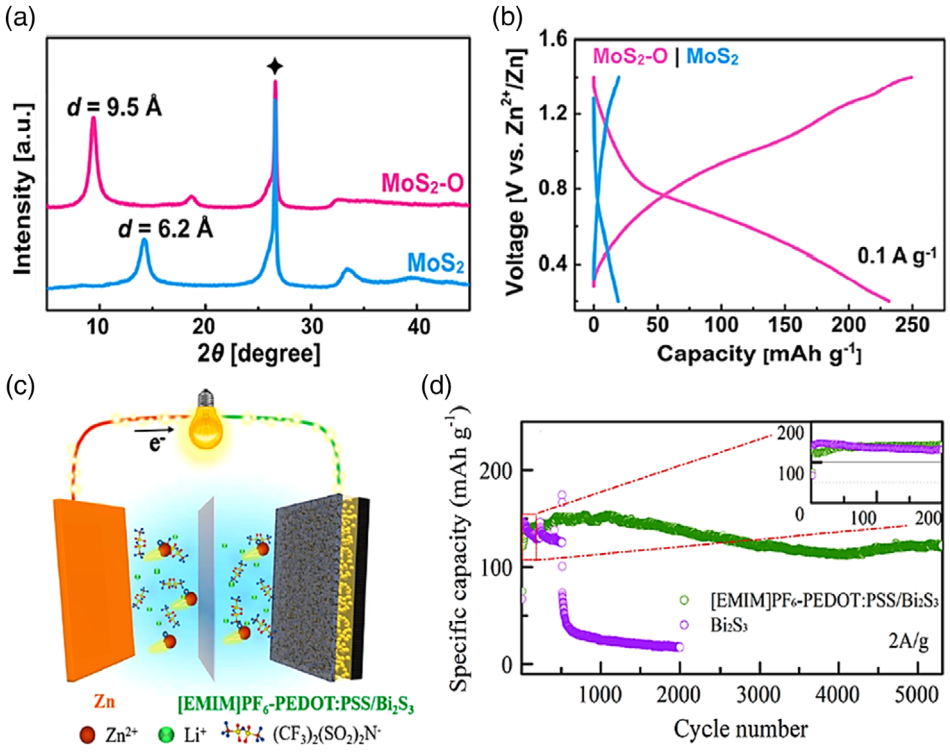

Figure 8. a) XRD patterns and b) GCD curves at 0.1 A g^{-1} of MoS_2—O and MoS_2 cathode in ZIBs. Reproduced with permission.[103] Copyright 2019, American Chemistry Society. c) Scheme of the Zn//[EMIM]PF_6-PEDOT:PSS/Bi_2S_3 cell, d) stability tests of Zn//Bi_2S_3 and Zn//[EMIM]PF_6-PEDOT:PSS/Bi_2S_3 batteries. Reproduced with permission.[107] Copyright 2019, American Chemistry Society.

nanosheets reduces the ion diffusion resistance, leading to faster reaction kinetics and lower intercalation energy barrier. This cathode delivers a specific capacity of 202.6 mAh g^{-1} at a rate of 0.1 A g^{-1}, and demonstrates good cycling stability with 98.6% retention after 600 cycles.

In addition to interlayer distance modification, defect engineering of MoS_2 has also been explored. Wang and co-workers prepared defect-rich MoS_{2-x} via a hydrothermal method followed by annealing under inert atmosphere.[105] The edge sites as well as sulfur vacancies enable a higher intercalation accessibility, resulting in significantly improved capacities of 138.6 mAh g^{-1} at 100 mA g^{-1} (corresponding to 0.36 Zn^{2+} per MoS_2) and excellent cyclability of 87.8% retention after 1000 cycles at 1 A g^{-1}. The defect-rich MoS_{2-x} displays another approach to improve the electrochemical performance of MoS_2. In another study, Chae et al. investigated the structural and electrochemical behavior of Mo_6S_8 when subjected to electrochemical intercalation of Zn^{2+}.[106] It was discovered that Mo_6S_8 experiences a two-step insertion at distinctly separate potential regions. The first stage occurs near 0.45–0.50 V versus Zn/Zn^{2+}, corresponding to occupation of Zn^{2+} in the interstitial Zn1 position surrounded by sulfur atoms, reducing Mo_6S_8 to $ZnMo_6S_8$. The second stage takes place at a voltage near 0.35 V, which corresponds to the conversion of $ZnMo_6S_8$ to $Zn_2Mo_6S_8$, in which Zn^{2+} ions are intercalated to the Zn2 sites. A significant portion of the inserted Zn^{2+} are trapped during the first discharge, resulting in a first-cycle irreversible capacity loss of 46 mAh g^{-1}.

4.3. Other Metal Sulfides

In 2019, Zhi group incorporated $[EMIM]PF_6$ (1-ethyl-3-methylimidazolium-hexafluorophosphate) ionic liquid and PEDOT:PSS (poly(3,4-ethylenedioxythiophene): poly(styrenesulfonate)) thin film with a Bi_2S_3 cathode by blade casting the ionic liquid solution onto the electrode surface to form a ZIBs composite cathode.[107] The ionic liquid containing PEDOT:PSS film enhances the conductivity of the composite, limits sulfur dissolution and stabilizes the electrolyte/electrode interface, resulting in a high specific capacity of 275 mAh g^{-1} at 0.3 A g^{-1} with excellent capacity retention of 95.3% over 5300 cycles (Figure 8c,d). Ex situ analyses of the cycled PEDOT:PSS/Bi_2S_3 reveal reversible conversion between Bi_2S_3 and hexagonal ZnS during the cycling process.

The highly reversible crystal structures and satisfactory discharge capacities of metal sulfides are favorable for ZIBs cathodes, but operating voltages of these materials are rather low for practical applications. Exploring novel metal sulfide chemistries with higher redox potentials may be the key to achieve breakthroughs. Recently, structural designs such as defect-engineering and interlayer space modification have been effective in improving the electrochemical performance. Composites beyond carbon materials should be investigated and developed for further performance optimization.

5. Organic Compounds

Organic cathode materials have gained significant attention for divalent ion batteries due to their affordable cost, sustainability, and environmental benignity.[22] Their inherently soft crystal structure and malleable lattice permit some degrees of molecular reorientation, which can free up active sites and promote reversible and facile interactions with hard divalent cations.[59] Organic materials also exhibit little intermolecular van der Waals force and relatively weak electrostatic repulsion toward incoming cations. Recently, investigations targeting C═O and N—H functional groups in organic materials as coordination sites for Zn^{2+} ions have emerged and brought interest toward the development of organic ZIBs cathodes.[108]

5.1. Quinone Compounds

Organic quinone compounds have been investigated as a possible replacement to inorganic ZIBs cathode materials mainly due to their high discharge capacity and relatively low polarization. In 2018, Chen and co-workers investigated the electrochemical performance of quinone compounds with carbonyl groups at various positions, including ortho-position 9,10-*PQ* (9,10-phenanthrenequinone, 1,2-*NQ* (1,2-naphthoquinone), para-position 9,10-*AQ* (9,10-anthraquinone), 1,4-*NQ* (1,4-naphthoquinone), and C4Q (calix[4]quinone) as cathodes in 3 M $Zn(CF_3SO_3)_2$ electrolyte.[109] From **Figure 9**b, it appears that quinone compounds with carbonyls in ortho-position generally exhibit lower capacities and higher voltage polarization than para-position carbonyls. This is possibly due to steric hindrance caused by ortho-positioned carbonyl, which restricts Zn^{2+} ions interaction with the primary active sites. Among them, C4Q displays the highest capacity of 335 mAh g^{-1}, which corresponds to three Zn^{2+} reacting with six carbonyl groups. The material also exhibits little voltage polarization of 70 mV at 0.02 A g^{-1} (Figure 9a), with capacity retention of 87% after 1000 cycles at 0.5 A g^{-1}.

Relations between the electrochemical performance of C4Q cathodes and the type of separator have also been investigated.[109] It was revealed that Zn_xC4Q formed during discharge can dissolve and release $C4Q^{2x-}$, which may travel to the anode and cause undesirable interactions and by-product generation. As such, the study adopted an ion selective Nafion membrane, which is only permeable to cations, and therefore improves the battery stability. The same group also applied poly(benzoquinonyl sulfide) (PBQS) as cathode, which achieves a discharge capacity of 203 mAh g^{-1} at 0.02 A g^{-1}.[110] The electrochemically active sites were confirmed as the C═O groups, and the overall redox reaction mechanism can be viewed as the reversible coordination of Zn^{2+} with the carbonyl functionality. In another example, Xia and co-workers assembled a PTO (pyrene-4,4,9,10-tetraone) cathode, which is inherently insoluble, with a conventional glass fiber separator to develop environmental-friendly flexible ZIBs.[111] The carbonyl groups on PTO are capable of reversibly coordinate with Zn^{2+}, enabling a high specific capacity of 336 mAh g^{-1} at 0.04 A g^{-1}. The ion-coordination reaction did not cause the PTO electrode to dissolve, and the fabricated cell therefore displays good rate capability and stability, achieving a capacity of 145 mAh g^{-1} at 3 A g^{-1} and a 70% capacity retention over 1000 cycles.

In 2018, Kundu et al. demonstrated a stable quinone *p*-chloranil (tetrachloro-1,4-benzoquinone) as an organic ZIBs cathode with capacity over 200 mAh g^{-1} and very low voltage polarization of 0.05 V.[59] Its malleable lattice permits rotation

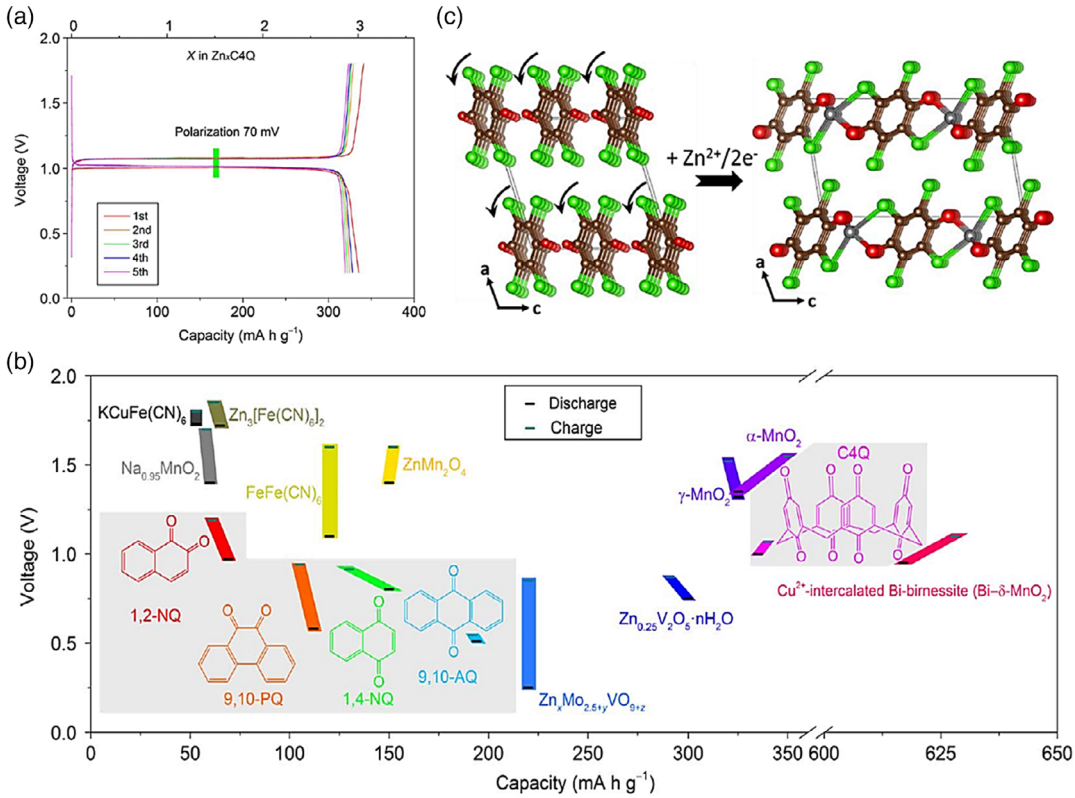

Figure 9. a) GCD of Zn-C4Q battery at 20 mA g^{-1}, with the upper *x* axis representing the Zn^{2+} uptake number, b) charge/discharge capacities and voltages of quinone compounds (1,2-NQ, 9,10-PQ, 1,4-NQ, 9,10-AQ, and C4Q) in fabricated aqueous ZIB compared to reported inorganic cathodes. Reproduced with permission.[109] Copyright 2018, American Association for the Advancement of Science. c) Structural models of *p*-chloranil (left) and Zn-*p*-chloranil (right) attained from DFT structural optimization results. Reproduced with permission.[59] Copyright 2018, American Chemical Society.

of the molecular column to form pathways for Zn^{2+} insertion, which diminishes volume change (–2.7%) during cycling (Figure 9c). Upon Zn^{2+} insertion, the *p*-chloranil molecule undergoes a reorientation to accommodate the inserted ions, leading to increased O—O and decreased Cl—Cl bond length. The change is caused by the coordination of Zn^{2+} with two chloranil molecules in adjacent columns, which forms a distorted tetrahedron. Furthermore, the housing of Zn^{2+} causes a reduction of the (010) and (100) plane d-spacing, in consequence of the improved structure packing, which can be detected by a small shrinkage of the unit cell volume.

As shown earlier, quinone compounds with C═O and/or C—O— functionalities are still hindered by their inherent solubility and instability, which demand proper mitigation strategies.[112] Recently, Stoddart and co-workers introduced phenanthrenequinone-based macrocycle (PQ-Δ) with robust triangular structure as a ZIBs cathode with superior layered structure and rigid geometry that achieves 99.9% capacity retention after 500 cycle.[113] The study reveals the co-insertion of Zn^{2+} ions and water molecules into the PQ-Δ cathode, which effectively diminishes the Zn^{2+} desolvation step and thus lowers the cathode/electrolyte interfacial resistance. Additionally, DFT results confirm the lowered desolvation energy by accommodating hydrated Zn^{2+} to enable high active site accessibility. Meanwhile, Wang and co-workers evaluated DTT (sulfur heterocyclic quinone dibenzo[*b*,*i*]thianthrene-5,7,12,14-tetraone) as ZIBs cathodes.[112] Using 2 M $ZnSO_4$ electrolyte, the cathode shows a superior reversible capacity of 210.9 mAh g^{-1} at 0.050 A g^{-1} at a high electrode loading of 5 mg cm^{-2}. It was demonstrated that DTT can accommodate both H^+ and Zn^{2+} simultaneously to form $DTT_2(H^+)_4(Zn^{2+})$, in which Zn^{2+} is bound to the C═O groups from the neighboring DTT molecules. Given the intrinsically low solubility of the discharged DTT, the DTT//Zn batteries exhibit an ultra-long cycle life over 23 000 with capacity retention up to 83.8%. Overall, these studies provided examples in designing the molecular structure and tailoring the ion coordination environment to improve the cyclability and redox activity.

5.2. Polyaniline Compounds

Recently, conductive polymers such as polyaniline (PANI) have been explored as organic cathodes for metal ion batteries and shown encouraging performance.[114] However, this material requires a highly acidic environment to generate adequate redox reactions, not compatible with zinc metal anode that rapidly dissolves in concentrated acid. In 2018, Sun and co-workers modified PANI by copolymerizing metanilic acid and aniline to form PANI-S and tested the resulting product as an aqueous ZIBs cathode.[115] The incorporated —SO_3^- functional groups serve as a dopant and proton reservoir to maintain high local H^+

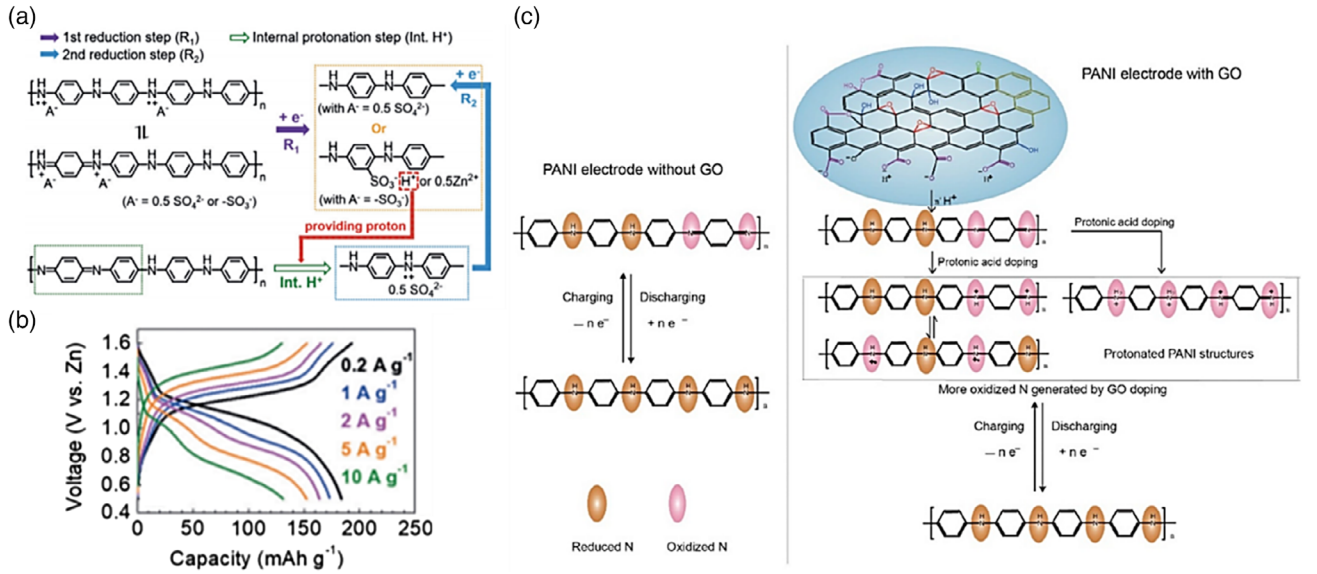

Figure 10. a) Scheme of proposed reduction mechanism after conditioning cycles, b) GCD curves of PANI-S cathode at different rates in aqueous ZIBs. Reproduced with permission.[115] Copyright 2018, Wiley-VCH. c) Scheme of energy storage mechanism of the prepared GO-doped PANI cathode. Reproduced with permission.[116] Copyright 2020, Elsevier.

concentration near the polymer backbone for optimal reaction kinetics. The proposed reduction process is demonstrated in **Figure 10**a, where half of the N in charged PANI-S is oxidized (—NH^+—, —N= or —NH^+=) and the protonated N are balanced by either —SO_3^- or SO_4^{2-} in the electrolyte. The protonated N species are more likely to accept electrons than non-protonated —N=. Therefore, they are first reduced to —NH— in the reduction process (R_1), which releases the external SO_4^{2-} to balance the charges. Meanwhile, the incorporated —SO_3^- remains on the polymer and interacts with either Zn^{2+} and H^+ cations in the electrolyte to create a low-pH environment near the polymer backbone. During this process, the oxidized —N= are internally protonated to —NH^+— by either H^+ interacting with the released —SO_3^- or H^+ attracted by the negatively charged electrode during reduction, which makes them available for reduction in the second step (R_2). Following such mechanism, the PANI-S delivers a high capacity of 180 mAh g^{-1} in 1 M $ZnSO_4$ (Figure 10b) and achieve a long lifespan over 2000 cycles at the current density of 10 A g^{-1} with nearly 100% Coulombic efficiency. Similarly, Li and co-workers discovered that graphene oxide (GO) with abundant oxygen groups can also serve as a local proton reservoir which can ease PANI protonation (Figure 10c).[116] The oxygen-containing functional groups of GO release H^+ in aqueous electrolyte, which enables GO as an organic acid. The study showed that a larger portion of N in the PANI backbone is protonated as a result of the GO incorporation, which enables higher charge transfer capacity during cycling.

5.3. Performance Optimization Strategies

5.3.1. Incorporation with Carbon Materials

Incorporating organic quinone cathodes with electronically conductive carbon materials has been investigated as an efficient approach to improve mechanical strength and electrochemical performances. In 2019, Liu and co-workers grafted cross-linked polydopamine (PDA) on conductive CNTs, which showed decent cyclability for over 500 cycles.[117] The reaction mechanism was identified to be redox reaction between the ortho-quinone and catechol of PDA accompanied by Zn^{2+} ion adsorption/desorption. In another study, Xu and co-workers developed cross-conjugated polycatechol (PC) with graphene by a hydrothermal reaction.[118] The hydroxyl groups on the composite are converted to carbonyl groups in the first cycle, which then coordinate with Zn^{2+} during discharge to form organometallic compounds of $C_6H_4O_2Zn$. The enolation reactions from ortho-positioned carbonyls and zinc ions can prevent the collapse of the material structure. Benefiting from the enhanced electronic conductivity and suitable zinc ion transport channels provided by graphene, the composite cathode shows a high specific capacity of 355 mAh g^{-1} at 50 mA g^{-1} and retains 74.4% of its original capacity after 3000 cycles at 1 A g^{-1}.

5.3.2. Nitrogen Substitution

In 2019, Shao and co-workers replaced the center O atom in the O=C—O—C=O moiety of NTCDA (1,4,5,8-naphthalenetetracarboxylic dianhydride) with N to synthesize NTCDI (1,4,5,8-naphthalene diimide).[119] The nitrogen substitution changes the electron distribution of C=O groups nearby and increases their likelihood to interact with Zn^{2+}, which optimizes the electrochemical performance. The improved active site utilization raises the discharge capacity of NTCDI to 240 mAh g^{-1} at 0.1 A g^{-1}, compared to 170 mAh g^{-1} for NTCDA. Meanwhile, the π-conjugation arrangement in NTCDI enables high structural integrity, allowing the material to maintain 73.7% of its capacity over 2000 cycles.

5.3.3. Combination of Redox-Active Sites

Abdul et al. first applied HqTp (hydroquinone based covalent organic framework) as a Zn^{2+} anchor for aqueous rechargeable ZIBs.[108] The C═O and N─H functionalities located in adjacent layers of HqTp provide inter-layer interactions with Zn^{2+} ions. Meanwhile, the well-defined honey-comb structure establishes pore with sizes near 1.5 nm, which facilitates rapid Zn^{2+} ion transport throughout the cathode. Benefiting from the aforementioned characteristics, HqTp can deliver a discharge capacity of 276 mAh g^{-1} at 125 mA g^{-1} with 95% capacity retained after 1000 cycles at 3.75 A g^{-1}. In another study, Stoddart and co-workers employed 2D conductive MOF $Cu_3(HHTP)_2$ as a ZIBs cathode.[120] Its large open crystal framework enables low interfacial resistance and high diffusion rates for the insertion of hydrated Zn^{2+} ions, resulting in a decent reversible capacity of 228 mAh g^{-1} at 0.05 A g^{-1}. Furthermore, the study proposed that intercalation pseudocapacitance is the primary working mechanism of $Cu_3(HTTP)_2$ with both the quinoid and copper atoms being the redox-active sites as shown in **Figure 11**.

5.3.4. Activation of Dual-Ion Redox

Advanced dual-ion redox reactions have been reported to enable batteries to reach higher operating voltage, rate capability, and superior cyclability.[121] In contrast to standard rocking-chair batteries that execute only cation de/intercalation, dual-ion batteries enable anion uptake to charge balance electron loss during oxidation, which would provide additional capacity. In 2018, Chen and co-workers developed aqueous Zn/PANI batteries in 1 M $Zn(CF_3SO_3)_2$ aqueous electrolyte[122] with cathodes suitable for Zn^{2+} and anion insertion/extraction (**Figure 12**a). Specifically, when charged, Zn^{2+} are first completely release from the cathode, then the cathode would then interact with $CF_3SO_3^-$ in the remaining charging process for charge compensation; the reverse would occur when the battery is discharged. As for the anode side, the Zn/Zn^{2+} redox would be the only targeted reaction occurring throughout the process. The batteries display a working voltage near 1.1 V and a long lifespan after 3000 cycles, showing capacity retention of 92% at 5 A g^{-1}. It should be noted that these batteries can be prepared into flexible soft-package or cable form, and exhibit excellent electrochemical performance at various bending states (Figure 12b). In 2019, Kundu and co-workers proposed BDB (1,4 bis(diphenylamino)benzene) as a novel organic material for dual-ion aqueous ZIBs cathodes.[123] As shown in Figure 12c, the two tertiary N centers in 1,4-bis (diphenylamino)benzene are oxidized/reduced in two steps during charge/discharge, and this redox reaction is paired with reversible attach/detachment of electrolyte anions to balance the charges. Worth noting, oxidized BDB is a decent catalyst for water oxidation, and this side reaction needs to be inhibited using highly concentrated "water-in-salt" electrolyte to ensure optimal Columbic efficiency (Figure 12d). In this electrolyte, the salt content is extremely high, to the point where free movement of water is inhibited by the ions. Thus, the battery operational voltage window can be widened to 0.4–2.1 V, allowing the BDB cathode to deliver a reversible discharge capacity of 125 mAh g^{-1} with an average potential of 1.25 V, corresponding to an energy density of ≈155 W h kg^{-1}. On another note, standard BDB is insoluble in the electrolyte, but BDB^{2+} may dissolve in concentrated electrolyte, which can be observed as a strong blue color on the separator. To address this issue, researchers have adapted CNC membranes with partially negatively charged functional groups to stabilize the oxidized product and suppress its dissolution, enabling the battery to achieve a capacity retention by of 75% after 1000 cycles.[123]

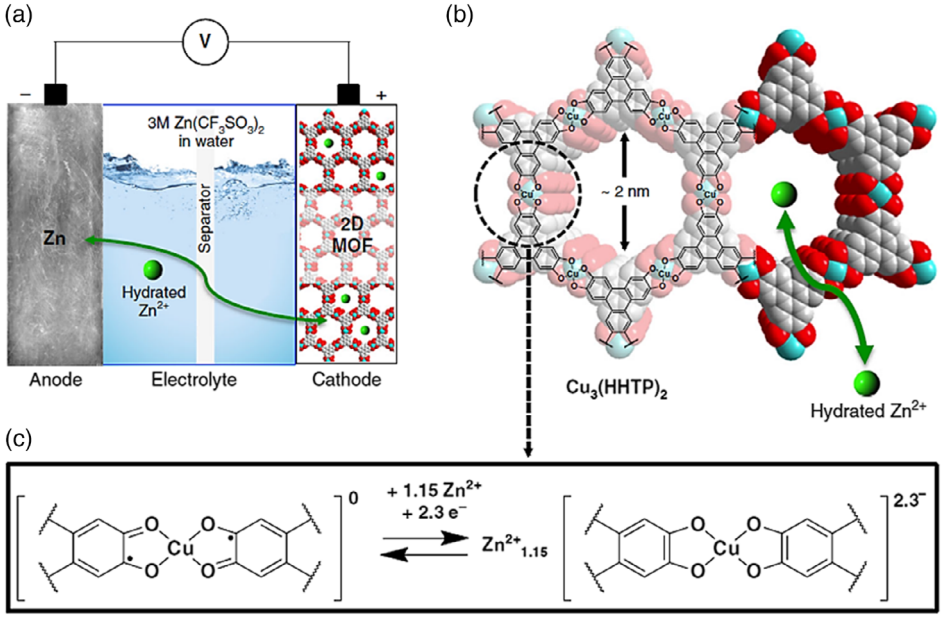

Figure 11. a) Scheme of rechargeable Zn-$Cu_3(HHTP)_2$ cell, b) structure of $Cu_3(HHTP)_2$, the cyan, gray, and red spheres represent Cu, C, and O atoms, c) expected redox reaction in Zn-$Cu_3(HHTP)_2$ cell. Reproduced with permission.[120] Copyright 2019, Springer Nature.

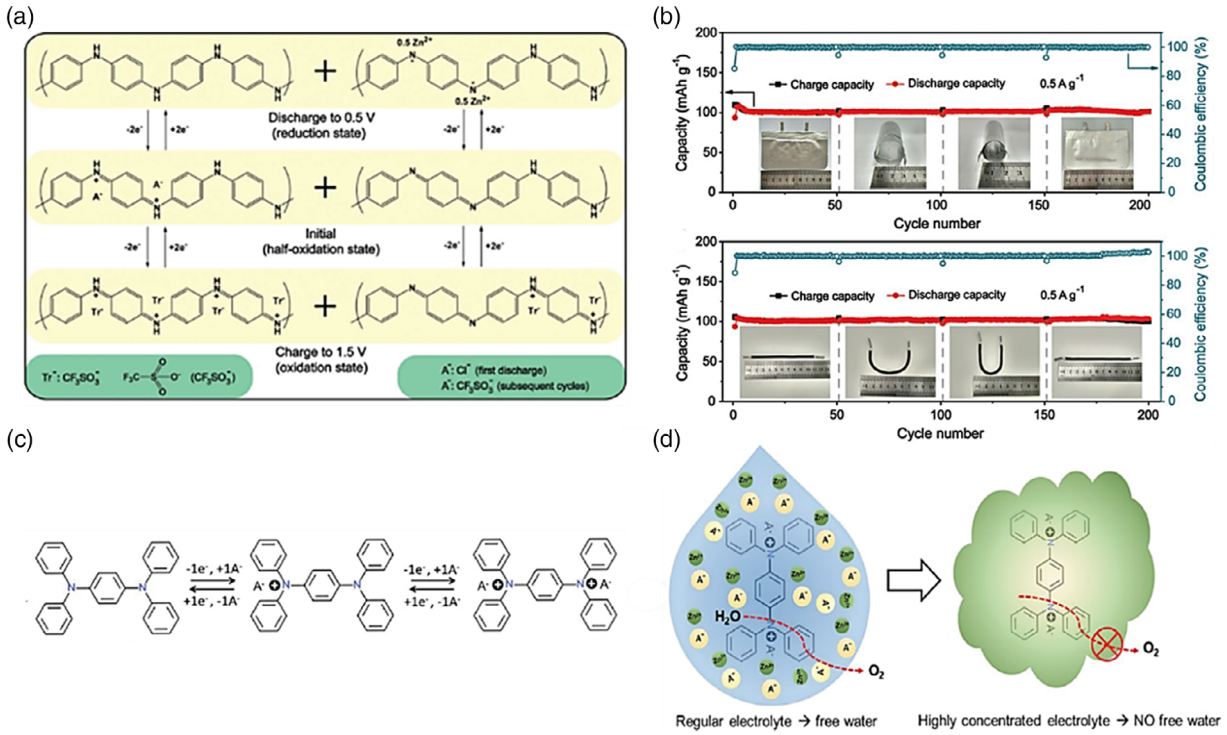

Figure 12. a) Scheme of proposed oxidation/reduction mechanism of PANI/CFs, b) cycling data of soft-packaged ZIB**s** and cable-type ZIBs at 500 mA g^{-1}. Inserted images are soft-packaged and cable-type batteries in diverse bending angles. Reproduced with permission.[122] Copyright 2018, Wiley-VCH. c) Scheme of two-step redox mechanism of BDB; A^-: OTf^-/$TFSI^-$, d) **s**chematic illustrating catalytic oxidation of free water by BDB^{2+} in regular aqueous electrolytes and highly concentrated ("water-in-salt") electrolyte. Reproduced with permission.[123] Copyright 2019, American Chemical Society.

6. Conclusion and Outlook

Research interests toward advanced cathode materials with specific advantages for rechargeable ZIBs are on the rise. In the earlier discussions, the advantages and drawbacks of novel ZIBs cathode materials are described and investigated systematically. Compared to Mn- and V- based maerials frequently explored for applications in ZIBs, certain cathodes discussed in this review have demonstrated discharge platforms with voltages that reach or exceed 1.8 V. Numerous examples with thousands of charge and discharge cycles have also been reported, with few exceeding ten thousands cycle that are far superior compared to Mn-based cathodes with weak cycling stability at high depth of discharge.[124] Specific electrochemical performance benchmarks of these cathode materials are compiled in **Figure 13** and **Table 1**. Based on this information, a brief summary and perspective regarding the current and future development of these materials are provided later.

First, among the different cathodes, PBAs display the highest discharge voltages (1.5−1.8 V), but their unsatisfactory discharge capacities restrict further increases in energy density. Currently, CoHCF is the only member in this family that achieves competitive capacities over 170 mAh g^{-1} with average voltages around 1.7 to 1.75 V.[77,88] Other PBAs such as ZnHCF and CuHCF still suffer from low discharge capacities below 100 mAh g^{-1}.[54,74,125] Researchers have attempted to apply mixed-metal HCFs and generate PBA-composites to increase the capacity.[78] Applications of

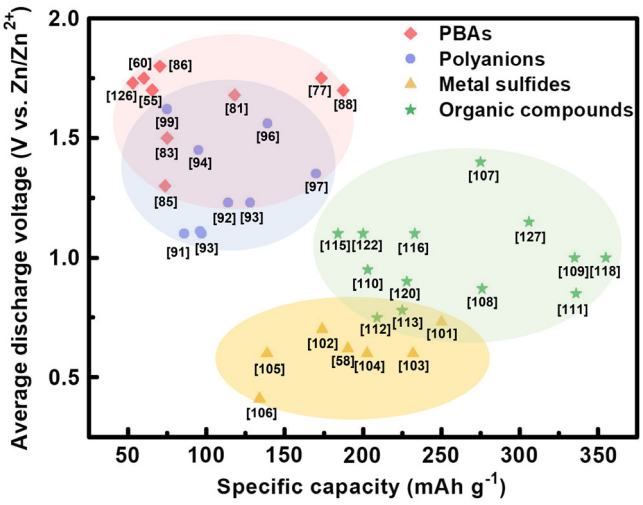

Figure 13. Average discharge voltages and specific capacity of ZIBs cathode materials in selected literatures. Red area represents PBAs, blue area represents polyanions, yellow area represents metal sulfides, and green area represents organic compounds.

hybrid aqueous electrolytes or ionic liquid electrolytes have also been effective in avoiding capacity decay.[126] Aside from these methods, possible routes for further improvement include

Table 1. Comparison of electrochemical performances of discussed cathode materials.

Cathode material	Voltage window (V vs Zn/Zn^{2+})	Electrolyte	Average operating voltage (V vs Zn/Zn^{2+})	Specific capacity [mAh g^{-1}]	Cycle performance	Ref.
ZnHCF	0.8–2.0	1 M $ZnSO_4$	1.7	65.4 at 0.06 A g^{-1}	76% after 100 cycles at 0.3 A g^{-1}	[55]
ZnHCF	0.8–2.0	3 M $ZnSO_4$	1.73	66.5 at 0.06 A g^{-1}	80% after 200 cycles at 0.3 A g^{-1}	[60]
ZnHCF	0–1.2 vs SCE	1 M $Zn(NO_3)_2$ 1 M KNO_3	0.84 vs SCE	66 at 0.3 A g^{-1}	73.3% after 100 cycles	[72]
ZnHCF	1.2–2.05	0.1 M $ZnSO_4$	1.75	62.5 at 0.042 A g^{-1}	81% after 10 cycles at 0.04 A g^{-1}	[126]
ZnHCF@MnO_2	1.4–1.9	0.5 M $ZnSO_4$	1.68	118 at 0.1 A g^{-1}	77% after 1000 cycles at 0.5 A g^{-1}	[81]
CuHCF	0.6–1.3 vs SHE	0.02 M $ZnSO_4$	1.73	53 at 0.06 A g^{-1}	96.3% after 100 cycles at 0.06 A g^{-1}	[72]
CuHCF	0.2–1.1 vs Ag/AgCl	0.02 M $ZnSO_4$	0.7 vs Ag/AgCl	55 at 0.06 A g^{-1}	97% after 200 cycles at 0.06 A g^{-1}	[75]
CuHCF	0–1.1 vs SCE	1 M $ZnSO_4$	0.65 vs SCE	56 at 0.02 A g^{-1}	77% after 20 cycles at 0.02 A g^{-1}	[74]
CuHCF	0.2–1.1 vs Ag/AgCl	0.1 M $ZnSO_4$	0.7 vs Ag/AgCl	53 at 1 C	56% after 1000 cycles at 1 C	[76]
CuHCF	1.4–2.1	1 M Na_2SO_4 0.01 M H_2SO_4	1.75	60 at 0.06 A g^{-1}	83% after 500 cycles at 0.3 A g^{-1}	[82]
CuHCF	0.4–1.3 vs NHE	0.1 M $Zn(ClO_4)_2$ 2 M $NaClO_4$	1 vs NHE	56 at 0.06 A g^{-1}	73% after 500 cycles at 0.3 A g^{-1}	[79]
CuHCF	1.4–2.3	1 M $(NH_4)_2SO_4$ 0. 1 M $ZnSO_4$	1.8	70.4 at 0.3 A g^{-1}	76.5% after 1000 cycles at 1.8 A g^{-1}	[86]
CuZnHCF	0.2–1.1 vs Ag/AgCl	0.02 M $ZnSO_4$	0.53 vs Ag/AgCl	53 at 0.085 A g^{-1}	85% after 1000 cycles	[78]
NiHCF	0.9–1.9	0.5 M Na_2SO_4 0.05 M $ZnSO_4$	1.5	75 at 0.1 A g^{-1}	81% after 1000 cycles at 0.5 A g^{-1}	[83]
CoHCF	0.7–2.0	4 M $Zn(OTf)_2$	1.75	173.4 at 0.3 A g^{-1}	100% after 2200 cycles at 3 A g^{-1}	[77]
CoHCF	0.4–2.1	2 M $Zn(BF_4)_2$	1.7	187.3 at 0.25 A g^{-1}	95% after 40000 cycles at 4 A g^{-1}	[88]
MnCoHCF	0–1.0 vs Ag/AgCl	1 M $Zn(ClO_4)_2$	0.77 vs Ag/AgCl	111 at 0.025 Ag^{-1}	93% after 100 cycles at 0.1 A g^{-1}	[80]
FeHCF	0.8–2.0	1.0 M $Zn(OAc)_2$	1.1	120 at 0.01 A g^{-1}	95% after 10 cycles at 0.01 A g^{-1}	[70]
NaFeHCF	0.8–2.0	1 M $(NH_4)_2SO_4$ 0.02 M $ZnSO_4$	1.3	73.6 at 0.25 A g^{-1}	92.1% after 2000 cycles at 2 A g^{-1}	[85]
KNiHCF	0.7–1.8	0.5 M $Zn(ClO_4)_2$ in acetonitrile	1.19	55.6 at 0.0112 A g^{-1}	96% after 35 cycles at 0.056 A g^{-1}	[87]
$Na_3V_2(PO_4)_3$/C	0.9–1.7	0.5 M $Zn(CH_3COO)_2$	1.1	97 at 0.05 A g^{-1}	74% after 100 cycles at 0.05 A g^{-1}	[91]
$Li_3V_2(PO_4)_3$/C	0.7–2.1	1 M Li_2SO_4/2 M $ZnSO_4$	1.23	128 at 0.2 C	85.4% after 200 cycles at 0.2 C	[93]
$Na_3V_2(PO_4)_3$/C	0.7–2.1	1 M Li_2SO_4/2 M $ZnSO_4$	1.11	96 at 0.2 C	84.1% after 200 cycles at 0.2 C	[93]
$Na_3V_2(PO_4)_3$/C	0.8–1.7	2 M $NaCH_3COO$ 1 M $Zn(CH_3COO)_2$	1.45	95 at 0.0468 A g^{-1}	72% after 1000 cycles at 3.5 A g^{-1}	[94]
$Na_3V_2(PO_4)_3$/rGO	0.6–1.8	2 M $Zn(CF_3SO_3)_2$	1.23	114 at 0.05 A g^{-1}	75% after 200 cycles at 0.5 A g^{-1}	[92]
$Na_3V_2(PO_4)_2F_3$/C	0.8–1.9	2 M $Zn(CF_3SO_3)_2$	1.62	75 at 0.08 A g^{-1}	95% after 4000 cycles at 1 A g^{-1}	[99]
$VOPO_4$	0.8–2.1	21 M LiTFSI1 M $Zn(Tr)_2$	1.56	139 at 0.05 A g^{-1}	93% after 1000 cycles at 1 A g^{-1}	[96]
$VOPO_4 \cdot nH_2O$	0.7–1.9	13 M $ZnCl_2$0.8 M H_3PO_4	1.35	170 at 0.1 A g^{-1}	92% after 500 cycles at 2 A g^{-1}	[97]
$VOPO_4$/ppy	0.58–1.7	1 M $Zn(CF_3SO_3)_2$	1.1	86 at 0.025 A g^{-1}	99% after 350 cycles at 0.1 A g^{-1}	[95]
Mo_6S_8	0.25–1	0.1 M $ZnSO_4$	0.41	134 at 0.0064 A g^{-1}	/	[106]
VS_2	0.4–1	1 M $ZnSO_4$	0.62	190.3 at 0.05 A g^{-1}	98% after 200 cycles at 0.5 A g^{-1}	[58]
VS_4/rGO	0.35–1.8	1 M $Zn(CF_3SO_3)_2$	0.73	250 at 0.2 A g^{-1}	93.3% after 165 cycles at 1 A g^{-1}	[101]
HCC-V_3S_4	0.5–1.5	2 M $ZnSO_4$	0.7	174 at 0.1 A g^{-1}	95% after 200 cycles at 0.5 A g^{-1}	[102]
MoS_2	0.2–1.4	3 M $Zn(CF_3SO_3)_2$	0.6	232 at 0.1 A g^{-1}	68% after 2000 cycles at 1 A g^{-1}	[103]
MoS_2	0.3–1.5	1 M $ZnSO_4$	0.6	202.6 at 0.1 A g^{-1}	98.6% after 600 cycles at 1 A g^{-1}	[104]
MoS_2	0.25–1.25	3 M $Zn(CF_3SO_3)_2$	0.6	138.6 at 0.1 A g^{-1}	87% after 1000 cycles at 1 A g^{-1}	[105]
[EMIM]PF_6 PEDOT:PSS/Bi_2S_3	0.1–2.3	1 M $Zn(TFSI)_2$ 21 M LiTFSI	1.4	275 at 0.3 A g^{-1}	95.3% after 5300 cycles at 2 A g^{-1}	[107]
C4Q	0.2–1.8	3 M $Zn(CF_3SO_3)_2$	1.0	335 at 0.02 A g^{-1}	87% after 1000 cycles at 0.5 A g^{-1}	[109]
PBQS	0.2–1.8	3 M $Zn(CF_3SO_3)_2$	0.95	203 at 0.02 A g^{-1}	86% after 50 cycles at 0.04 A g^{-1}	[110]
p-chloranil	0.8–1.4	1 M $Zn(OTf)_2$	1.1	170 at 0.0434 A g^{-1}	70% after 200 cycles at 0.217 A g^{-1}	[59]
PQ-Δ	0.25–1.6	3 M $Zn(CF_3SO_3)_2$	0.78	225 at 0.03 A g^{-1}	99.9% after 500 cycles at 0.15 A g^{-1}	[113]
DTT	0.3–1.4	2 M $ZnSO_4$	0.75	209 at 0.05 A g^{-1}	83.8% after 23000 cycles at 2 A g^{-1}	[112]
HqTp	0.2–1.8	3 M $ZnSO_4$	0.87	276 at 0.125 A g^{-1}	95% after 1000 cycles at 3.75 A g^{-1}	[108]
$Cu_3(HTTP)_2$	0.5–1.3	3 M $Zn(CF_3SO_3)_2$	0.9/0.65	228 at 0.05 A g^{-1}	75% after 500 cycles at 4 A g^{-1}	[120]
PTO	0.36–1.46	2 M $ZnSO_4$	0.85	336 at 0.04 A g^{-1}	70% after 1000 cycles at 3 A g^{-1}	[111]

Table 1. Continued.

Cathode material	Voltage window (V vs Zn/Zn^{2+})	Electrolyte	Average operating voltage (V vs Zn/Zn^{2+})	Specific capacity [mAh g^{-1}]	Cycle performance	Ref.
NTCDI	0.35–1.25	2 M $ZnSO_4$	0.5	240 at 0.04 A g^{-1}	73.7% after 2000 cycles at 1 A g^{-1}	[119]
PDA/CNT	0.3–1.4	3.3 M $ZnSO_4$	0.8	126.2 at 0.02 A g^{-1}	96% after 500 cycles at 0.2 A g^{-1}	[117]
PC/rGO	0.2–1.9	3 M $ZnSO_4$	1.0	355 at 0.05 A g^{-1}	66.2% after 2000 cycles at 1 A g^{-1}	[118]
PANI-S	0.5–1.6	1 M $ZnSO_4$	1.1	184 at 0.2 A g^{-1}	84.6% after 2000 cycles at 10 A g^{-1}	[115]
PANAC//CC	0.7–1.5	3 M NH_4Cl/2 M $ZnCl_2$	1.15	306.3 at 0.28 A g^{-1}	73% after 1100 cycles at 0.56 A g^{-1}	[127]
PANI/GO	0.5–1.6	2.5 M $Zn(CF_3SO_3)_2$	1.1	233 at 0.1 A g^{-1}	78.7% after 2500 cycles at 3 A g^{-1}	[116]
PANI	0.5–1.5	1 M $Zn(CF_3SO_3)_2$	1.1	200 at 0.05 A g^{-1}	92% after 3000 cycles at 5 A g^{-1}	[122]
BDB	0.4–2.1	19 M $LiN(SO_3\ CF_3)_2$/1 M $Zn(CF_3SO_3)_2$	1.25	125 at 0.026 A g^{-1}	75% after 1000 cycles at 0.39 A g^{-1}	[123]

surface chemistry alteration, foreign ion doping and forming composites with other high capacity cathode materials. The investigation of alternative electrolytes to suppress zinc dendrite formation and promote PBA intercalation reversibility should also be encouraged.

Compared to PBAs, polyanions such as NASICONs and $VOPO_4$ exhibit moderate average voltages of 1.1−1.6 V with acceptable capacities near 100 mAh g^{-1},[91–93,97] whereas chevrel phase compounds and metal sulfides deliver capacities over 200 mAh g^{-1} with low average voltages below 0.8 V.[102,104] Recent development efforts in hybrid aqueous electrolyte optimization, interlayer spacing adjustment and defect-engineering have resolved various structural stability issues, drastically improving the cycle life of these materials to upward of 5000 cycles. However, further capacity and voltage optimization are still required, which may be achieved via proper activation and refinement of the corresponding anion redox processes for both cathode materials. Advanced characterizations with high resolution can be utilized to detect variances in crystal structure at the atomic scale and their correlation with electrochemical performances, which may provide inspiration for material design.

In contrast, organic cathodes have frequently achieve high reversible capacities over 300 mAh g^{-1} and decent operating voltages near 1.0−1.3 V, resulting in energy densities comparable to Mn or V-based cathodes.[111] In addition, they also exhibit low polarizability and superb cyclability as their redox reaction does not involve bulk crystallogical transformation. Currently, investigations of N—H and C═O functionalities as active sites have just begun, and low electronic conductivity of these organic materials is the primary limiting factor. It is anticipated that with further improvements in charge transports and discoveries of new active sites suitable for zinc ion interaction, organic cathodes hold great promise in exceeding common ZIBs cathodes and realizing wide-spread adoption.

Other than the commonly reported cationic insertion/extraction reactions, novel mechanisms including reversible oxygen/sulfur redox and anionic redox reactions have also been applied in ZIBs. These two distinct reactions can enhance the battery capacity and enlarge the voltage window, resulting in higher battery energy density. As the existing ZIBs still primarily rely on the cationic redox reactions, advanced reaction mechanisms would provide an alternative route to achieve systems with superior performances. For industry applications, development of solid-state ZIBs and biosafe ZIBs are encouraged. For instance, $ZnSO_4$/PVA gel and PAM with F77 skin hydrogel have been applied as electrolytes for quasi-solid-state flexible batteries. Bio-ionic liquid water electrolyte can also be used to synthesize bio-degradable ZIBs.

In summary, novel ZIBs cathode materials with inherent benefits and practical promises call for deeper investigation and development. In addition to structural and morphology modification, electrolyte optimization, flexible solid-state system designs, and insight into their working/degradation mechanisms are also encouraged to pave a bright future for ZIBs.

Acknowledgements

This work was sponsored by Natural Sciences and Engineering Research Council of Canada (NSERC), University of Waterloo and Waterloo Institute for Nanotechnology.

Conflict of Interest

The authors declare no conflict of interest.

Keywords

cathode materials, electrolytes, mechanisms, zinc-ion batteries

Received: July 31, 2020
Revised: September 7, 2020
Published online:

[1] S. Chu, A. Majumdar, *Nature* **2012**, *488*, 294.
[2] A. Manthiram, *Nat. Commun.* **2020**, *11*, 1.
[3] X. Wang, Y. L. Ding, Y. P. Deng, Z. Chen, *Adv. Energy Mater.* **2020**, *10*, 1903864.
[4] T. Or, S. W. Gourley, K. Kaliyappan, A. Yu, Z. Chen, *Carbon Energy* **2020**, *2*.
[5] G. L. Zhu, C. Z. Zhao, J. Q. Huang, C. He, J. Zhang, S. Chen, L. Xu, H. Yuan, Q. Zhang, *Small* **2019**, *15*, 1805389.
[6] L. Đorđević, F. Arcudi, M. Prato, *Nat. Protoc.* **2019**, *14*, 2931.
[7] T.T.D. Nguyen, S. Abada, A. Lecocq, J. Bernard, M. Petit, G. Marlair, S. Grugeon, S. Laruelle, *World Electric Vehicle Journal* **2019**, *10*, 79.

[8] H. Xu, C. Peng, Y. Yan, F. Dong, H. Sun, J. Yang, S. Zheng, *Carbon Energy* **2019**, *1*, 276.
[9] M. Li, C. Wang, Z. Chen, K. Xu, J. Lu, *Chem. Rev.* **2020**, *120*, 6783.
[10] J. Wu, Y. Cao, H. Zhao, J. Mao, Z. Guo, *Carbon Energy* **2019**, *1*, 57
[11] S. Chen, D. Wang, Y. Zhao, D. Wang, *Small Methods* **2018**, *2*, 1800038.
[12] J. Meng, Q. Pang, L. Mai, *Matter* **2020**, *2*, 1363
[13] J. Fu, R. Liang, G. Liu, A. Yu, Z. Bai, L. Yang, Z. Chen, *Adv. Mater.* **2019**, *31*, 1805230.
[14] G. Li, F. Lu, X. Dou, X. Wang, D. Luo, H. Sun, A. Yu, Z. Chen, *J. Am. Chem. Soc.* **2020**, *142*, 3583
[15] W. Shin, J. Lu, X. Ji, *Carbon Energy* **2019**, *1*, 165.
[16] X. Y. Fan, J. Han, Y. L. Ding, Y. P. Deng, D. Luo, X. Zeng, Z. Jiang, L. Gou, D. L. Li, Z. Chen, *Adv. Energy Mater.* **2019**, *9*, 1900673.
[17] H. Yuan, J. Nai, H. Tian, Z. Ju, W. Zhang, Y. Liu, X. Tao, X.W.D. Lou, *Sci. Adv.* **2020**, *6*, eaaz3112.
[18] Y. P. Deng, Z. G. Wu, R. Liang, Y. Jiang, D. Luo, A. Yu, Z. Chen, *Adv. Funct. Mater.* **2019**, *29*, 1808522.
[19] R. Paul, Q. Dai, C. Hu, L. Dai, *Carbon Energy* **2019**, *1*, 19.
[20] K. Kaliyappan, T. Or, Y. P. Deng, Y. Hu, Z. Bai, Z. Chen, *Adv. Funct. Mater.* **2020**, *30*, 1910251.
[21] S. Lou, Y. Zhao, J. Wang, G. Yin, C. Du, X. Sun, *Small* **2019**, *15*, 1904740.
[22] G. Fang, J. Zhou, A. Pan, S. Liang, *ACS Energy Lett.* **2018**, *3*, 2480.
[23] M. Zhang, W. Liu, R. Liang, R. Tjandra, A. Yu, *Sustainable Energy & Fuels* **2019**, *3*, 2499.
[24] M. Li, X. Bi, R. Wang, Y. Li, G. Jiang, L. Li, C. Zhong, Z. Chen, J. Lu, *Matter* **2020**, *2*, 32.
[25] M. M. Huie, D. C. Bock, E. S. Takeuchi, A. C. Marschilok, K. J. Takeuchi, *Coord. Chem. Rev.* **2015**, *287*, 15.
[26] P. Padigi, G. Goncher, D. Evans, R. Solanki, *J. Power Sources* **2015**, *273*, 460.
[27] Q. Li, N. J. Bjerrum, *J. Power Sources* **2002**, *110*, 1.
[28] T. Cai, L. Zhao, H. Hu, T. Li, X. Li, S. Guo, Y. Li, Q. Xue, W. Xing, Z. Yan, *Energy Environ. Sci.* **2018**, *11*, 2341.
[29] J. Ming, J. Guo, C. Xia, W. Wang, H. N. Alshareef, *Mater. Sci. Eng., R* **2019**, *135*, 58.
[30] D. Selvakumaran, A. Pan, S. Liang, G. Cao, *J. Mater. Chem. A* **2019**, *7*, 18209.
[31] C. Li, X. Zhang, W. He, G. Xu, R. Sun, *J. Power Sources* **2020**, *449*, 227596.
[32] X. Wang, F. Wang, L. Wang, M. Li, Y. Wang, B. Chen, Y. Zhu, L. Fu, L. Zha, L. Zhang, *Adv. Mater.* **2016**, *28*, 4904.
[33] F. Cheng, J. Chen, X. Gou, P. Shen, *Adv. Mater.* **2005**, *17*, 2753.
[34] T. Shoji, M. Hishinuma, T. Yamamoto, *J. Appl. Electrochem.* **1988**, *18*, 521.
[35] C. Xu, B. Li, H. Du, F. Kang, *Angew. Chem. Int. Ed.* **2012**, *51*, 933.
[36] H. Li, C. Xu, C. Han, Y. Chen, C. Wei, B. Li, F. Kang, *J. Electrochem. Soc.* **2015**, *162*, A1439.
[37] Y.-P. Deng, R. Liang, G. Jiang, Y. Jiang, A. Yu, Z. Chen, *ACS Energy Lett.* **2020**, *5*, 1665.
[38] P. He, Q. Chen, M. Yan, X. Xu, L. Zhou, L. Mai, C.-W. Nan, *EnergyChem* **2019**, 100022.
[39] Y. Zhao, Y. Zhu, X. Zhang, *InfoMat* **2020**, *2*, 237.
[40] F. Wan, Z. Niu, *Angew. Chem. Int. Ed.* **2019**, *58*, 16358.
[41] N. Zhang, F. Cheng, J. Liu, L. Wang, X. Long, X. Liu, F. Li, J. Chen, *Nat. Commun.* **2017**, *8*, 1.
[42] B. Wu, G. Zhang, M. Yan, T. Xiong, P. He, L. He, X. Xu, L. Mai, *Small* **2018**, *14*, 1703850.
[43] S. Zhao, B. Han, D. Zhang, Q. Huang, L. Xiao, L. Chen, D. G. Ivey, Y. Deng, W. Wei, *J. Mater. Chem. A* **2018**, *6*, 5733.
[44] Y. Li, S. Wang, J. R. Salvador, J. Wu, B. Liu, W. Yang, J. Yang, W. Zhang, J. Liu, J. Yang, *Chem. Mater.* **2019**, *31*, 2036.
[45] S.-D. Han, S. Kim, D. Li, V. Petkov, H. D. Yoo, P. J. Phillips, H. Wang, J. J. Kim, K. L. More, B. Key, *Chem. Mater.* **2017**, *29*, 4874.
[46] M. H. Alfaruqi, V. Mathew, J. Gim, S. Kim, J. Song, J. P. Baboo, S. H. Choi, J. Kim, *Chem. Mater.* **2015**, *27*, 3609.
[47] N. Zhang, Y. Dong, M. Jia, X. Bian, Y. Wang, M. Qiu, J. Xu, Y. Liu, L. Jiao, F. Cheng, *ACS Energy Lett.* **2018**, *3*, 1366.
[48] J. Ding, Z. Du, L. Gu, B. Li, L. Wang, S. Wang, Y. Gong, S. Yang, *Adv. Mater.* **2018**, *30*, 1800762.
[49] P. Hu, M. Yan, T. Zhu, X. Wang, X. Wei, J. Li, L. Zhou, Z. Li, L. Chen, L. Mai, *Acs Appl. Mater. Interfaces* **2017**, *9*, 42717.
[50] M. Yan, P. He, Y. Chen, S. Wang, Q. Wei, K. Zhao, X. Xu, Q. An, Y. Shuang, Y. Shao, *Adv. Mater.* **2018**, *30*, 1703725.
[51] F. Wan, L. Zhang, X. Dai, X. Wang, Z. Niu, J. Chen, *Nat. Commun.* **2018**, *9*, 1.
[52] F. Ming, H. Liang, Y. Lei, S. Kandambeth, M. Eddaoudi, H. N. Alshareef, *ACS Energy Lett.* **2018**, *3*, 2602.
[53] D. Xu, H. Wang, F. Li, Z. Guan, R. Wang, B. He, Y. Gong, X. Hu, *Adv. Mater. Interfaces* **2019**, *6*, 1801506.
[54] R. Y. Wang, C. D. Wessells, R. A. Huggins, Y. Cui, *Nano Lett.* **2013**, *13*, 5748.
[55] L. Zhang, L. Chen, X. Zhou, Z. Liu, *Adv. Energy Mater.* **2015**, *5*, 1400930.
[56] S. Li, Y. Dong, L. Xu, X. Xu, L. He, L. Mai, *Adv. Mater.* **2014**, *26*, 3545.
[57] Y. Cheng, L. Luo, L. Zhong, J. Chen, B. Li, W. Wang, S. X. Mao, C. Wang, V. L. Sprenkle, G. Li, *Acs Appl. Mater. Interfaces* **2016**, *8*, 13673.
[58] P. He, M. Yan, G. Zhang, R. Sun, L. Chen, Q. An, L. Mai, *Adv. Energy Mater.* **2017**, *7*, 1601920.
[59] D. Kundu, P. Oberholzer, C. Glaros, A. Bouzid, E. Tervoort, A. Pasquarello, M. Niederberger, *Chem. Mater.* **2018**, *30*, 3874.
[60] L. Zhang, L. Chen, X. Zhou, Z. Liu, *Sci. Rep.* **2015**, *5*, 1.
[61] F. Ma, Q. Li, T. Wang, H. Zhang, G. Wu, *Sci. Bull.* **2017**, *62*, 358.
[62] M. Song, H. Tan, D. Chao, H. J. Fan, *Adv. Funct. Mater.* **2018**, *28*, 1802564.
[63] M. H. Wong, Z. Zhang, X. Yang, X. Chen, J. Y. Ying, *Chem. Commun.* **2015**, *51*, 13674.
[64] Y. Lu, L. Wang, J. Cheng, J. B. Goodenough, *Chem. Commun.* **2012**, *48*, 6544.
[65] Y. You, X.-L. Wu, Y.-X. Yin, Y.-G.J.E. Guo, E. Science, **2014**, *7*, 1643.
[66] G. He, L. F. Nazar, *ACS Energy Lett* **2017**, *2*, 1122.
[67] T. Tojo, Y. Sugiura, R. Inada, Y. Sakurai, *Electrochim. Acta* **2016**, *207*, 22.
[68] L. Reed, S. Ortiz, M. Xiong, E. Menke, *Chem. Commun.* **2015**, *51*, 14397.
[69] L. Chen, J. Bao, X. Dong, D. G. Truhlar, Y. Wang, C. Wang, Y. Xia, *ACS Energy Lett.* **2017**, *2*, 1115.
[70] Z. Liu, G. Pulletikurthi, F. Endres, *Acs Appl. Mater. Interfaces* **2016**, *8*, 12158.
[71] B. Wang, Y. Han, X. Wang, N. Bahlawane, H. Pan, M. Yan, Y. Jiang, *Iscience* **2018**, *3*, 110.
[72] R. Trócoli, F. La Mantia, *ChemSusChem* **2015**, *8*, 481.
[73] G. Ni, B. Han, Q. Li, Z. Ji, B. Huang, C. Zhou, *ChemElectroChem* **2016**, *3*, 798.
[74] Z. Jia, B. Wang, Y. Wang, *Mater. Chem. Phys.* **2015**, *149*, 601.
[75] G. Kasiri, R. Trócoli, A. B. Hashemi, F. La Mantia, *Electrochim. Acta* **2016**, *222*, 74.
[76] J. Lim, G. Kasiri, R. Sahu, K. Schweinar, K. Hengge, D. Raabe, F. La Mantia, C. Scheu, *Chemistry* **2019**, *26*.
[77] L. Ma, S. Chen, C. Long, X. Li, Y. Zhao, Z. Liu, Z. Huang, B. Dong, J. A. Zapien, C. Zhi, *Adv. Energy Mater.* **2019**, *9*, 1902446.
[78] G. Kasiri, J. Glenneberg, A. B. Hashemi, R. Kun, F. La Mantia, *Energy Storage Mater.* **2019**, *19*, 360.
[79] R. Trócoli, G. Kasiri, F. La Mantia, *J. Power Sources* **2018**, *400*, 167.

[80] N. Kuperman, M. Hopkins, S. Olson, G. Goncher, D. Evans, R. Solanki, *IEEE 13th Nanotechnology Materials and Devices Conf.* IEEE, Piscataway, NJ **2018**, pp. 1.
[81] K. Lu, B. Song, Y. Zhang, H. Ma, J. Zhang, *J. Mater. Chem. A* **2017**, *5*, 23628.
[82] T. Gupta, A. Kim, S. Phadke, S. Biswas, T. Luong, B. J. Hertzberg, M. Chamoun, K. Evans-Lutterodt, D. A. Steingart, *J. Power Sources* **2016**, *305*, 22.
[83] K. Lu, B. Song, J. Zhang, H. Ma, *J. Power Sources* **2016**, *321*, 257.
[84] X. Wu, Y. Qi, J. J. Hong, Z. Li, A. S. Hernandez, X. Ji, *Angew. Chem. Int. Ed.* **2017**, *56*, 13026.
[85] C. Li, D. Zhang, F. Ma, T. Ma, J. Wang, Y. Chen, Y. Zhu, L. Fu, Y. Wu, W. Huang, *ChemSusChem* **2019**, *12*, 3732.
[86] C. Li, J. Wu, F. Ma, Y. Chen, L. Fu, Y. Zhu, Y. Zhang, P. Wang, Y. Wu, W. Huang, *ACS Appl. Energy Mater.* **2019**, *2*, 6984.
[87] M. S. Chae, J. W. Heo, H. H. Kwak, H. Lee, S.-T. Hong, *J. Power Sources* **2017**, *337*, 204.
[88] L. Ma, S. Chen, N. Li, Z. Liu, Z. Tang, J. A. Zapien, S. Chen, J. Fan, C. Zhi, *Adv. Mater.* **2020**, *32*, 1908121.
[89] Z. Liu, P. Bertram, F. Endres, *J. Solid State Electrochem.* **2017**, *21*, 2021.
[90] S. S. Soni, K. B. Fadadu, A. Gibaud, *Langmuir* **2012**, *28*, 751.
[91] G. Li, Z. Yang, Y. Jiang, C. Jin, W. Huang, X. Ding, Y. Huang, *Nano Energy* **2016**, *25*, 211.
[92] P. Hu, T. Zhu, X. Wang, X. Zhou, X. Wei, X. Yao, W. Luo, C. Shi, K. A. Owusu, L. Zhou, L. Mai, *Nano Energy* **2019**, *58*, 492.
[93] H. Zhao, C. Hu, H. Cheng, J. Fang, Y. Xie, W. Fang, T. Doan, T. Hoang, J. Xu, P. Chen, *Sci. Rep.* **2016**, *6*, 25809.
[94] S. Islam, M. H. Alfaruqi, D. Y. Putro, V. Mathew, S. Kim, J. Jo, S. Kim, Y. K. Sun, K. Kim, J. Kim, *ChemSusChem* **2018**, *11*, 2239.
[95] V. Verma, S. Kumar, W. Manalastas Jr, J. Zhao, R. Chua, S. Meng, P. Kidkhunthod, M. Srinivasan, *ACS Appl. Energy Mater.* **2019**, *2*, 8667.
[96] F. Wan, Y. Zhang, L. Zhang, D. Liu, C. Wang, L. Song, Z. Niu, J. Chen, *Angew. Chem. Int. Ed.* **2019**, *58*, 7062.
[97] H. Y. Shi, Y. Song, Z. Qin, C. Li, D. Guo, X. X. Liu, X. Sun, *Angew. Chem. Int. Ed.* **2019**, *58*, 16057.
[98] W. Song, Z. Wu, J. Chen, Q. Lan, Y. Zhu, Y. Yang, C. Pan, H. Hou, M. Jing, X. Ji, *Electrochim. Acta* **2014**, *146*, 142.
[99] W. Li, K. Wang, S. Cheng, K. Jiang, *Energy Storage Mater.* **2018**, *15*, 14.
[100] Z. Hu, L. Wang, K. Zhang, J. Wang, F. Cheng, Z. Tao, J. Chen, *Angew. Chem. Int. Ed.* **2014**, *53*, 12794.
[101] H. Qin, Z. Yang, L. Chen, X. Chen, L. Wang, *J. Mater. Chem. A* **2018**, *6*, 23757.
[102] S. Liu, X. Chen, Q. Zhang, J. Zhou, Z. Cai, A. Pan, *Acs Appl. Mater. Interfaces* **2019**, *11*, 36676.
[103] H. Liang, Z. Cao, F. Ming, W. Zhang, D. H. Anjum, Y. Cui, L. Cavallo, H. N. Alshareef, *Nano Lett.* **2019**, *19*, 3199.
[104] H. Li, Q. Yang, F. Mo, G. Liang, Z. Liu, Z. Tang, L. Ma, J. Liu, Z. Shi, C. Zhi, *Energy Storage Mater.* **2019**, *19*, 94.
[105] W. Xu, C. Sun, K. Zhao, X. Cheng, S. Rawal, Y. Xu, Y. Wang, *Energy Storage Mater.* **2019**, *16*, 527.
[106] M. S. Chae, J. W. Heo, S.-C. Lim, S.-T. Hong, *Inorg. Chem.* **2016**, *55*, 3294.
[107] Y. Zhao, L. Ma, Y. Zhu, P. Qin, H. Li, F. Mo, D. Wang, G. Liang, Q. Yang, W. Liu, C. Zhi, *ACS Nano* **2019**, *13*, 7270.
[108] A. Khayum, M. Ghosh, V. Vijayakumar, A. Halder, M. Nurhuda, S. Kumar, M. Addicoat, S. Kurungot, R. Banerjee, *Chem. Sci.* **2019**, *10*, 8889.
[109] Q. Zhao, W. Huang, Z. Luo, L. Liu, Y. Lu, Y. Li, L. Li, J. Hu, H. Ma, J. Chen, *Sci. Adv.* **2018**, *4*, eaao1761.
[110] G. Dawut, Y. Lu, L. Miao, J. Chen, *Inorg. Chem. Front.* **2018**, *5*, 1391.
[111] Z. Guo, Y. Ma, X. Dong, J. Huang, Y. Wang, Y. Xia, *Angew. Chem.* **2018**, *130*, 11911.
[112] Y. Wang, C. Wang, Z. Ni, Y. Gu, B. Wang, Z. Guo, Z. Wang, D. Bin, J. Ma, Y. Wang, *Adv. Mater.* **2020**, *32*, 2000338.
[113] K. W. Nam, H. Kim, Y. Beldjoudi, T.-W. Kwon, D. J. Kim, J. F. Stoddart, *J. Am. Chem. Soc.* **2020**, *142*, 2541.
[114] H. Gao, L. Xue, S. Xin, J. B. Goodenough, *Angew. Chem. Int. Ed.* **2018**, *57*, 5449.
[115] H. Y. Shi, Y. J. Ye, K. Liu, Y. Song, X. Sun, *Angew. Chem.* **2018**, *130*, 16597.
[116] W. Du, J. Xiao, H. Geng, Y. Yang, Y. Zhang, E. H. Ang, M. Ye, C. C. Li, *J. Power Sources* **2020**, *450*, 227716.
[117] X. Yue, H. Liu, P. Liu, *Chem. Commun.* **2019**, *55*, 1647.
[118] S. Zhang, W. Zhao, H. Li, Q. Xu, *ChemSusChem* **2020**, *13*, 188.
[119] X. Wang, L. Chen, F. Lu, J. Liu, X. Chen, G. Shao, *ChemElectroChem* **2019**, *6*, 3644.
[120] K. W. Nam, S. S. Park, R. Dos Reis, V. P. Dravid, H. Kim, C. A. Mirkin, J. F. Stoddart, *Nat. Commun.* **2019**, *10*, 1.
[121] I. A. Rodríguez-Pérez, X. Ji, *ACS Energy Lett.* **2017**, *2*, 1762.
[122] F. Wan, L. Zhang, X. Wang, S. Bi, Z. Niu, J. Chen, *Adv. Funct. Mater.* **2018**, *28*, 1804975.
[123] H. Glatz, E. Lizundia, F. Pacifico, D. Kundu, *ACS Appl. Energy Mater.* **2019**, *2*, 1288.
[124] H. Pan, Y. Shao, P. Yan, Y. Cheng, K. S. Han, Z. Nie, C. Wang, J. Yang, X. Li, P. Bhattacharya, *Nature Energy* **2016**, *1*, 1.
[125] M. S. Chae, S.-T. Hong, *Batteries* **2019**, *5*, 3.
[126] B. Tang, L. Shan, S. Liang, J. Zhou, *Energy Environ. Sci.* **2019**, *12*, 3288.
[127] P. Li, Z. Fang, Y. Zhang, C. Mo, X. Hu, J. Jian, S. Wang, D. Yu, *J. Mater. Chem. A* **2019**, *7*, 17292.

Aiping Yu is a professor in the Department of Chemical Engineering at the University of Waterloo, Ontario, Canada. She received her Ph.D. from the University of California, Riverside in 2007. Her research mainly involves the synthesis, functionalization, and application of carbon-based nanostructured materials for photocatalysts and energy storage and conversion such as supercapacitors, lithium-ion batteries, and metal–air batteries.

Zhongwei Chen obtained his Ph.D. from the University of California, Riverside in 2007. He is Canada Research Chair Professor (Tier 1) in Advanced Materials for Clean Energy at the University of Waterloo, a Fellow of the Canadian Academy of Engineering, and vice president of International Academy of Electrochemical Energy Science (IAOEES). His research focuses on the development of advanced materials for energy storage and electrocatalysis and their applications in metal–air batteries, fuel cells, and lithium-ion batteries.